vaccines

MDPI

Article

A Sequential Benznidazole–Vaccine–Benznidazole Regimen Enhances Therapeutic Efficacy Against Chronic *Trypanosoma cruzi* Infection in Mice

Paula Cacik [1], Estefanía Prochetto [1], Ulises Cha [1], María Florencia Pacini [2], Camila Bulfoni Balbi [2], Brenda Dinatale [2], Genaro Francisco Díaz [1], Florencia Belén González [2], Cecilia Farre [2], Ana Rosa Pérez [2] and Iván Sergio Marcipar [1,*]

[1] Laboratorio de Tecnología Inmunológica Facultad de Bioquímica y Ciencias Biológicas, Universidad Nacional del Litoral, Consejo Nacional de Investigaciones Científicas y Técnicas (LTI-FBCB-CONICET), Santa Fe 3000, Argentina; paula.cacik@gmail.com (P.C.); eprochetto@fbcb.unl.edu.ar (E.P.); ucha@ful.unl.edu.ar (U.C.); genarof.diaz@gmail.com (G.F.D.)

[2] Instituto de Inmunología Clínica y Experimental de Rosario (IDICER-CONICET-UNR) and CIPREB, Facultad de Ciencias Médicas, Universidad Nacional de Rosario, Rosario 2000, Argentina; flo.pacini@hotmail.com (M.F.P.); camibulfoni@gmail.com (C.B.B.); brenda.dinatale@gmail.com (B.D.); gonzalez@idicer-conicet.gob.ar (F.B.G.); cfarre.cipreb@gmail.com (C.F.); perezanarosa50@gmail.com (A.R.P.)

* Correspondence: imarcipr@gmail.com

Abstract

Background/Objectives: Chronic Chagas cardiomyopathy (CCC), caused by *Trypanosoma cruzi* (*T. cruzi*), remains a major public health challenge and a leading cause of heart failure, with this chronic stage representing the period when most patients are diagnosed and require clinical intervention. However, the efficacy of the available parasiticidal drugs, benznidazole (BZL) and nifurtimox during chronic infection is limited and new therapeutic approaches are needed. In this study, we evaluated a novel sequential chemo-immunotherapeutic strategy (BZL → Vac → BZL) designed to shorten benznidazole treatment duration to minimize drug-related adverse effects by leveraging the synergistic potential of both treatments. **Methods:** BALB/c mice chronically infected with *T. cruzi* were used as model. A long-term sequential regimen was evaluated and compared 190 days post-infection with uninfected, untreated infected (Tc), monotherapy (BZL or TSNt-ISPA vaccine), and combined (Vac → BZL) controls. The sequential treatment consisted of an initial short cycle of oral BZL, three subcutaneous immunizations with the TSNt-ISPA vaccine, and a final BZL booster. Cardiac parasite load and cytokine expression (qPCR), inflammation and fibrosis (histopathology), electrocardiograms (ECG), specific antibodies (ELISA), and splenic cellular response (flow cytometry) were analyzed. **Results:** The BZL-Vac → BZL scheme significantly reduced cardiac parasite load, achieving undetectability in some animals. Combined therapies (Vac → BZL and BZL → Vac → BZL) significantly attenuated myocardial inflammation and fibrosis, improving P-wave duration and the QTc interval. The sequential treatment induced a robust Th1-associated humoral response (IgG2a) and a balanced cellular profile, uniquely increasing splenic IL-10-producing $CD4^+$ T cells, TNF-α-producing $CD8^+$ T cells, and cardiac IL-10 and Foxp3 expression. **Conclusions:** The temporal integration of fractionated benznidazole and TSNt-ISPA immunotherapy protects myocardial integrity and function through an effector immune response under strict regulatory control.

Keywords: chagas cardiomyopathy; chronic infection; therapeutic vaccine; chemo-immunotherapy; trans-sialidase

Check for updates

Academic Editor: Ola Winqvist

Received: 13 October 2026
Revised: 5 November 2026
Accepted: 12 November 2026
Published: 17 November 2026

Copyright: © 2026 by the authors. Licensee MDPI, Basel, Switzerland. This article is an open access article distributed under the terms and conditions of the Creative Commons Attribution (CC BY) license.

1. Introduction

Chagas disease, caused by the hemoflagellate protozoan *Trypanosoma cruzi* (*T. cruzi*), remains a major global public health challenge, affecting an estimated 6–7 million people worldwide [1]. Owing to human migration and globalization, the disease has spread beyond its original endemic regions in Latin America and is now recognized as a global health concern [2,3]. Although the acute phase is often asymptomatic or presents with only mild clinical manifestations, approximately 30–40% of infected individuals progress to the chronic stage, developing chronic Chagas cardiomyopathy (CCC) [2,4]. CCC is the leading cause of infectious heart failure and non-ischemic cardiomyopathy in Latin America and is characterized by severe arrhythmias, thromboembolic events, and sudden cardiac death [3,5].

Currently, etiological treatment of Chagas disease relies on the nitroheterocyclic drugs benznidazole (BZL) and nifurtimox [2,5,6]. Although BZL is highly effective during the acute phase of infection, achieving parasitological cure rates of up to 80–100%, its efficacy in eliminating the parasite and preventing disease progression during the chronic phase remains markedly limited [5,7]. This limited therapeutic efficacy is influenced by several factors, including the complex biology and the strain of the parasite, as well as the poor tolerability and the high incidence of adverse effects, which frequently lead to treatment discontinuation [5,6,8,9]. Recent studies have shown that, during *in vivo* infection, *T. cruzi* amastigotes can spontaneously enter a dormant or quiescent state [10–12]. In this non-replicative state, the parasites markedly reduce their metabolic activity, enabling them to evade the action of trypanocidal drugs, whose activity depends on activation by parasite nitroreductases, and to survive prolonged drug exposure [10,11]. Consequently, these latent tissue reservoirs may serve as a source of parasite recrudescence following the discontinuation of conventional treatment.

In this scenario, therapeutic vaccination has emerged as a potential complementary strategy to BZL treatment for Chagas disease. By enhancing *T. cruzi*-specific immune responses, these vaccines could improve parasite control, reduce the risk of disease progression, and potentially allow the use of shorter or lower-dose drug regimens, thereby limiting treatment-associated adverse effects [13].

However, in addition to the intrinsic challenges posed by the parasite, chronic *T. cruzi* infection induces profound dysregulation of the host immune system. Persistent antigen exposure over time drives the clonal exhaustion of parasite-specific CD8 T cells [14]. This exhausted phenotype is characterized by a hierarchical loss of key effector functions, including cytokine production, reduced proliferative capacity, and the progressive co-expression of multiple inhibitory receptors [14].

In addition, the persistence of dormant parasite populations may reduce the effectiveness of BZL, as these metabolically quiescent forms are less susceptible to drug-mediated killing [10]. Concomitant immune exhaustion may further impair parasite clearance, thereby creating a negative feedback loop that favors long-term persistence and limits treatment efficacy [15,16]. Because therapeutic vaccination relies on reinvigorating or enhancing parasite-specific immune responses, we hypothesize that pre-existing T-cell dysfunction or exhaustion may limit its ability to achieve effective parasite control.

To overcome the limitations of drug monotherapy, the development of therapeutic vaccines in combination with chemotherapy (chemo-immunotherapy) has emerged as a highly promising strategy [3]. Building on this rationale, available preclinical studies have demonstrated that combining trypanocidal drugs with therapeutic vaccines—either concomitantly or sequentially—enhances parasite control, leading to greater reductions in tissue burden and cardiac damage than single-agent therapies [5,17–20]. Previous approaches, however, have varied widely in drug exposure, vaccination timing, and delivery order. For instance,

our group evaluated a strategy consisting of vaccination with a recombinant Nt fragment of the *T. cruzi* antigen Trans-sialidase (TSNt), formulated with the ISCOMATRIX-like adjuvant ISPA, followed by prolonged BZL treatment [17]. These approaches have differed substantially in the timing, duration, and relative order of chemotherapy and vaccination. Despite these advances, the optimal timing and sequencing of chemotherapy and vaccination remain unresolved, particularly regarding how best to address active parasite replication, persistent parasite populations, and infection-induced immune dysfunction.

In *T. cruzi* infection, mice chronically infected and successfully treated with BZL showed a reprogramming of the immune response towards an increase in T cells with a central memory phenotype that allows high protection against a challenge compared to untreated mice [21–23]. This effect was also observed in infected and treated humans [24]. More notably, it has been described in experimental models of infection that an active effector immune response mediated by IFN-γ, TNF-α, and IL-12 is required to increase efficacy of BZL treatment [25,26]. Taking into account the link between a favorable effect of BZL for the immune response and the efficacy of BZL treatment, in this study, we hypothesized that a sequential chemo-immunotherapeutic strategy (BZL → Vac → BZL) would maximize the complementary and potentially synergistic effects of chemotherapy and vaccination. An initial course of BZL was expected to reduce parasite burden and antigenic stimulation, thereby promoting a more effective parasite-specific immune response, thereby creating a favorable immunological environment for subsequent immunization with the recombinant TSNt + ISPA vaccine. The vaccine-induced immune response would then strengthen the control of residual or reactivated parasites, while a second course of BZL would target parasites that persisted or resumed active replication. This reciprocal interaction was expected to provide greater therapeutic efficacy than either treatment alone, while allowing shorter and better-tolerated treatment courses and preserving myocardial structure and function.

Based on this hypothesis, we first evaluated whether a short course of BZL, potentially allowing adverse effects to be avoided, could reduce parasite burden while simultaneously improving the immune system in infected mice. We then assessed whether this treatment scheme was effective in controlling chronic infection in a BALB/c mouse model chronically infected with the Tulahuen strain of *T. cruzi*.

2. Materials and Methods

2.1. Expression and Purification of TSNt Antigen

The recombinant TSNt antigen, a 35 kDa amino-terminal fragment of the *T. cruzi* Trans-sialidase (aa 63 to 346, GenBank accession AJ276679.1) lacking the C-terminal SAPA repeats, was expressed and purified as previously described [17]. Briefly, the antigen sequence containing an N-terminal His-tag was expressed using the pET-28a(+) vector system (Novagen™, EMD Biosciences, Madison, WI, USA) in *Escherichia coli* BL21 (DE3) cells. Protein production was induced with 0.1 mM IPTG overnight at room temperature under constant stirring. Expression was verified by 15% denaturing SDS-PAGE and visualized by Coomassie Blue staining. For scale-up, a 100 mL LB culture was harvested and lysed by cold sonication using a Vibra-Cell (Sonics & Materials Inc., Newtown, CT, USA). Since the TSNt fragment was obtained as insoluble inclusion bodies, the pellet was resuspended in PBS/urea 8 M. Purification was performed by affinity chromatography on Ni-NTA agarose columns (Invitrogen™, Carlsbad, CA, USA) using an imidazole gradient (20–500 mM). Purified protein fractions were pooled, concentrated using Vivaspin® 20 centrifugal concentrators (Sartorius Stedim Biotech GmbH, Göttingen, Germany; MWCO 10,000 Da) at 8000 *g*, and quantified by the bicinchoninic acid (BCA) method at 562 nm using BSA as a standard.

2.2. Animals and Experimental Infection Model

BALB/c female mice (6 to 8 weeks old) were obtained from the Centro de Medicina Comparada (ICIVET-CONICET, UNL, Esperanza, Argentina) with certified specific health and sanitary status for laboratory animals. Experimental protocols complied with institutional guidelines and were approved by the Advisory Committee of Ethics and Research Safety (CAESI) of the Facultad de Bioquímica y Ciencias Biológicas, UNL, Santa Fe, Argentina (Resolution no. CE2018-42-08/31/2018). Animals were housed in a vivarium under controlled conditions at 22 °C with a 12 h light/dark cycle, and food and water were available ad libitum. Mice underwent a formal acclimatization period of 14 days prior to experimental infection. Humane endpoints were established prior to the study: animals showing severe distress or body weight loss exceeding 30% relative to baseline were to be humanely euthanized. In this experimental cohort, all animals maintained clinical stability throughout the chronic phase, and no premature euthanasia or exclusions were required.

T. cruzi blood trypomastigotes (Tulahuen strain, DTU-VI), maintained by serial passages in suckling Cbi mice, were obtained from peripheral blood (CIPREB-FCM-UNR, Rosario, Argentina). To establish the chronic infection model, BALB/c mice were infected at day 0 by intradermal inoculation of 1000 viable blood trypomastigotes into the left footpad, in a final volume of 10 µL of sterile physiological saline solution. Infection was confirmed at day 14 post-infection (pi) by direct microscopic analysis of peripheral blood. In this model, parasitemia peaks at 2–3 weeks pi and is no longer detectable by microscopy after 6 weeks pi (day 42 pi) [27,28]. The chronic phase was defined by the absence of circulating parasites [29–31], and treatments were therefore started at day 52 pi, during this phase.

Following parasitemia confirmation, animals were randomly assigned to experimental groups by simple lottery (drawing lots), allocating one cage per experimental group prior to the onset of therapeutic interventions. All cages were placed adjacently under identical environmental conditions (temperature, ventilation, and lighting), so cage position was not rotated. To minimize potential confounders, animal handling, therapeutic administrations, and endpoint sampling and measurements (including ECG recordings and euthanasia) were performed in a randomized sequence across cages. The sample size for each group is detailed in Sections 2.3 and 2.4, and was determined according to the housing capacity of the cages used in the experiments.

2.3. Evaluation of Short-Term Benznidazole Treatment as an Immunomodulator

To evaluate the immunomodulatory potential of a shortened chemotherapy regimen compared to therapeutic vaccination, an exploratory proof-of-concept study was performed (Figure 1a,b). At day 52 pi, infected mice were allocated into three experimental cohorts: the Tc* group ($n = 5$), consisting of infected and untreated control mice receiving phosphate-buffered saline (PBS) as vehicle control; the BZL* group ($n = 6$), treated orally with a suboptimal dose of BZL at 100 mg/kg/day for 7 consecutive days (from days 52 to 59 pi) (Figure 1a); and the Vac* group ($n = 5$), receiving therapeutic vaccination alone via three subcutaneous doses of the TSNt + ISPA formulation (10 µg TSNt + 3 µL ISPA in a final volume of 100 µL PBS) administered on days 52, 62, and 72 pi (Figure 1b). BZL at 100 mg/kg/day is the standard dose in murine models of *T. cruzi* infection [32,33]; however, in our BALB/c-Tulahuen chronic model, a 30-day course of this dose does not achieve parasitological cure [17]. A shorter 7-day course was therefore used to limit drug exposure.

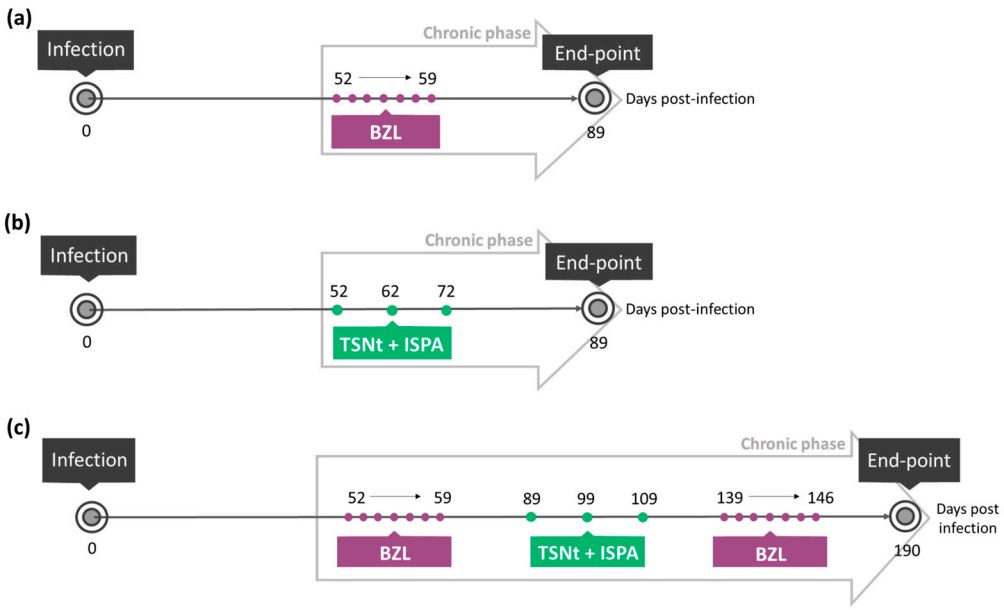


Figure 1. Chronology and experimental protocols evaluated in the chronic *T. cruzi* infection model. (**a**) Short-course oral Benznidazole (BZL, 100 mg/kg/day) monotherapy protocol, administered daily for 7 consecutive days starting at day 52 post-infection (pi); (**b**) therapeutic immunization protocol consisting of three subcutaneous doses of the TSNt-ISPA vaccine (10 µg of TSNt antigen and 3 µL of ISPA adjuvant per dose) administered at days 52, 62, and 72 pi. For both monotherapeutic schemes, the experimental endpoint was set at day 89 pi; (**c**) sequential chemo-immunotherapy protocol (BZL → Vac → BZL) consisting of an initial short course of oral BZL (from days 52 to 59 pi), followed by three subcutaneous immunizations with the TSNt-ISPA vaccine (at days 89, 99, and 109 pi), and a final oral BZL booster (from days 139 to 146 pi), with the study endpoint at day 190 pi.

On day 89 pi, all animals were anesthetized with a ketamine–xylazine mixture and euthanized by cervical dislocation to collect biological samples for subsequent immunological, parasitological, and histological analyses.

2.4. Evaluation of the Sequential Chemo-Immunotherapeutic Protocol BZL → Vac → BZL

To evaluate the efficacy of a sequential chemo-immunotherapeutic scheme, mice were distributed into the following groups: NI: uninfected and untreated control ($n = 6$); Tc: infected and untreated mice ($n = 7$); BZL: infected mice treated with two short cycles of BZL ($n = 7$); Vac: infected mice immunized with the TSNt-ISPA vaccine ($n = 7$); Vac → BZL: infected mice treated with the vaccine followed by a single cycle of BZL ($n = 7$); and BZL → Vac → BZL: infected mice treated with the sequential scheme (BZL + Vaccine + BZL, $n = 8$).

The sequential protocol was administered as follows (Figure 1c): a first short cycle of BZL (100 mg/kg/day, oral) was administered for 7 consecutive days starting at day 52 pi. One month later (days 89, 99, and 109 pi), the mice were immunized subcutaneously with the TSNt-ISPA vaccine formulation described above. Finally, a second 7-day cycle of BZL was administered starting one month after the last vaccine dose (day 139 pi). At day 190 pi, all animals were euthanized following the same procedure to collect biological samples for subsequent analyses. All treatments in the other groups followed the schedule of the sequential protocol, omitting the components indicated for each group.

2.5. Parasitological, Histological, ECG, and Immunological Assays

2.5.1. Histological Analysis

Hearts were removed at the end of the experiment (day 190 pi) and fixed in PBS/4% formalin. Tissues were embedded in paraffin and 5 µm sections were obtained. Sections were subsequently stained with hematoxylin and eosin (H&E) to evaluate inflammatory infiltrates and tissue damage, and with picrosirius red to analyze tissue fibrosis. The intensity of myocardial inflammation was classified into mild (discrete infiltrate with damage to few fibers), moderate (involvement of 3 to 5 muscle fibers), or severe (extensive infiltrates with destruction of multiple fibers). Fibrosis was equivalently categorized into mild, moderate, or severe based on the size and number of compromised fibers. Based on these categories, a scoring system was established to quantify both inflammation and fibrosis: normal = 0, mild = 1, moderate = 2, and severe = 3, as previously reported [27,34,35].

2.5.2. Quantification of Parasite Load in Heart

Heart parasite load was determined by quantitative PCR (qPCR) from tissue samples collected at sacrifice. Total DNA was isolated by traditional phenol–chloroform–isoamyl alcohol extraction. Briefly, transverse heart sections were disaggregated in lysis buffer (10 mM Tris-HCl, pH 7.6; 0.1 M NaCl; 10 mM EDTA; 0.5% SDS; 300 µg/mL proteinase K; Sigma, St. Louis, MO, USA) at 55 °C for 2 h, extracted with phenol–chloroform–isoamyl alcohol (25:24:1), and precipitated with cold ethanol. DNA templates were resuspended in sterile water and adjusted to 125 ng/µL.

The qPCR reactions were performed using HOT FIREPol EvaGreen qPCR Mix Plus (Solis BioDyne OÜ, Tartu, Estonia) in a StepOne™ Real-Time PCR Systems instrument (Applied Biosystems, Foster City, CA, USA). Specific primers targeting *T. cruzi* kDNA were used: S36 (5′-GGT TCG ATT GGG GTT GGT G-3′) and S67rev (5′-GAA CCC CCC TCC CAA AAC C-3′). The *T. cruzi* quantification curve was generated as previously described [17]. A standard curve for murine DNA quantification was constructed using specific primers for the murine TNF-α gene, as described by Cummings and Tarleton (2003) [36]. Parasite load was expressed as equivalent parasites per 250 ng of murine DNA, based on the standard curves provided in Figure A1 (Appendix A). The limit of detection (LOD) was defined as the lowest concentration of the standard curve amplified in all replicates: 0.01 parasite equivalents per 250 ng of DNA. Lower concentrations were not tested, so the actual LOD may be lower. Samples without amplification were considered not detected and assigned a value of zero. Each run included a no-template control (water added in the room containing the reaction mixture), a negative control (genomic DNA from an uninfected mouse) and a positive control (*T. cruzi* genomic DNA).

2.5.3. Electrocardiograms (ECGs)

At 190 days post-infection (pi), electrocardiographic recordings were performed in mice from all experimental groups under anesthesia with a ketamine/xylazine solution (100 mg/kg ketamine and 10 mg/kg xylazine) adjusted to body weight, as previously described [17,27,35]. Cardiac electrical activity was recorded using a mouse-adapted electrocardiographic system (CardioCom, Paraná, Argentina). ECG recordings were analyzed using the CC7DerS-Vet software (version 1.0.4; CardioCom, Paraná, Argentina), provided by the equipment manufacturer. The following parameters were evaluated: heart rate, P-wave duration, PR interval, QRS complex duration, and QT interval. The QT interval was corrected for heart rate (QTc) according to the formula described by Mitchell et al. (1998) [37].

2.5.4. Specific Antibody Detection

Specific total IgG, IgG1 and IgG2a antibodies were measured by indirect ELISA in plasma collected at the end of each study (day 89 pi in the short-term study; day 190 pi in the sequential study) [17,35]. Heparinized blood was centrifuged at 2000 rpm, and plas-ma was stored at −20 °C until analysis. Maxisorp plates (Nunc-Immuno, Thermo Fisher Scientific, Roskilde, Denmark) were coated overnight at 4 °C with 0.5 µg/well of recombinant TSNt or *T. cruzi* total homoge-nate (TH) in carbonate–bicarbonate buffer (0.05 M, pH 9.6). After washing with PBS–Tween 20 (0.05%) and blocking with 5% skim milk in PBS (1 h, 37 °C), plasma diluted 1:100 in PBS containing 1% skim milk was added in duplicate (1 h, 37 °C). Bound anti-bodies were detected using HRP-conjugated goat anti-mouse IgG, IgG1 or IgG2a (1:10,000; Abcam Cambridge, UK), incubated for 1 h at 37 °C, followed by TMB substrate (Invitrogen, Carlsbad, CA, USA). The reaction was stopped with sulfuric acid, and absorbance was measured at 450 nm using an ELISA microplate reader (Bio-Tek Instruments, Winooski, VT, USA). Results were expressed as a reactivity index (sample OD/cut-off), with the cut-off defined as the mean OD of non-infected (NI) control samples plus two standard deviations.

2.5.5. Cardiac Cytokine and Transcription Factor Profiling by RT-qPCR

Total RNA was extracted from a transverse section of heart tissue homogenized in TRI-Reagent® (Sigma-Aldrich, St. Louis, MO, USA) and reverse-transcribed using RevertAid Reverse Transcriptase (Thermo Fisher Scientific, Vilnius, Lithuania), as previously described [27,35]. Transcripts of IFN-γ, IL-17a, IL-10, Foxp3, T-bet, RORγt and GAPDH were quantified using a StepOnePlus Real-Time PCR System (Applied Biosystems, Waltham, MA, USA) and 5× HOT FIREPol® EvaGreen® qPCR Mix Plus with ROX (Solis BioDyne, Tartu, Estonia). Cy-cling consisted of 15 min at 95 °C followed by 40 cycles of 95 °C for 15 s, annealing at 59–62 °C and extension at 72 °C for 20 s, with fluorescence acquired at the end of each exten-sion step and specificity checked by melting curve analysis. Relative expression levels were calculated using an individual standard curve for each gene and normalized to GAPDH. Comparable amplification efficiencies between target and reference genes were verified. The specific primers used are listed in Table 1.

Table 1. Primers used for cardiac cytokine and transcription factor profiling by RT-qPCR.

Gene	Forward (5′-3′)	Reverse (5′-3′)
IFN-γ	AGACAATCAGGCCATCAGCAAC	CTCATTGAATGCTTGGCGCTG
IL-17a	CAAAGCTCAGCGTGTCCAAA	CTTCCCAGATCACAGAGGGATA
IL-10	CAAGCCTTATCGGAAATGATCCA	CCTTGTAGACACCTTGGTCTTG
Foxp3	AAAGGAGAAGCTGGGAGCTATG	GTGGCTACGATGCAGCAAGAG
T-bet	AGCTCACCAACAACAAGGGG	CTGCGTTCTGGTAGGCAGTC
RORγt	AGCAGTGTAATGTGGCCTACTCC	TGCATGTAGACTGTCCCTCTG
GAPDH	GAAGGTCGGTGTGAACGGAT	CGTTGAATTTGCCGTGAGTGGA

2.5.6. Flow Cytometry Analysis

To characterize the antigen-specific cellular immune response, splenocytes were isolated from mice at the end of each study (day 89 or day 190 pi). Spleens were mechanically disrupted to obtain single-cell suspensions, and red blood cells were lysed using an ammonium chloride (NH4Cl) solution. Fresh splenocytes were resuspended in RPMI 1640 medium (Gibco™, Thermo Fisher Scientific, Grand Island, NY, USA) supplemented with 10% fetal bovine serum (FBS), 100 U/mL penicillin, 100 µg/mL streptomycin (Gibco™, Thermo Fisher Scientific, Grand Island, NY, USA), and 0.4 mM 2-mercaptoethanol. To enhance antigen presentation and subsequent T-cell activation, splenocytes were seeded at

a density of 0.5×10^6 cells/mL in 48-well plates (Nunc™, Thermo Fisher Scientific, Roskilde, Denmark) and co-cultured with activated DCs pulse-loaded with 10 µg/mL of sterile *T. cruzi* TH. For the evaluation of intracellular cytokine production, the co-culture was stimulated for a total period of 15 h. This protocol included an initial 6 h incubation step, followed by an additional 9 h incubation in the presence of protein transport inhibitors (BD GolgiStop™, BD Pharmingen, San Diego, CA, USA) to induce cytoplasmic cytokine accumulation.

T-cell activation status, cytotoxic potential, and cytokine profiles were evaluated using fluorochrome-conjugated antibodies against CD4 (APC), CD8 (PerCP), CD44 (FITC), CD107a (PE), IFN-γ (PE or APC), IL-10 (PerCP; Invitrogen, Carlsbad, CA, USA), and TNF-α (FITC; Miltenyi Biotec, Bergisch Gladbach, Germany). The immunolabeling procedure began with the incubation of surface antibodies (anti-CD4, anti-CD8, anti-CD44, or anti-CD107a) for 30 min. Cells were then washed and resuspended in a fixation and permeabilization solution (BD Cytofix/Cytoperm™, BD Pharmingen, San Diego, CA, USA) for 30 min at 4 °C. After a final wash step, cells were incubated with the intracellular monoclonal antibodies anti-IFN-γ (PE or APC), anti-IL-10/PerCP (Invitrogen, Carlsbad, CA, USA), or anti-TNF-α/FITC (Miltenyi Biotec, Bergisch Gladbach, Germany). All other reagents and surface antibodies were purchased from BD Pharmingen™ (San Diego, CA, USA).

A target of 1×10^5 events per sample was acquired on the BD Accuri™ C6 Plus cytometer (BD Biosciences, Ann Arbor, MI, USA). Gating strategies and frequency analyses were performed using FlowJo software (version 10.8.1; FlowJo LLC, Ashland, OR, USA).

Gates were set using fluorescence-minus-one controls as illustrated in Figure A2 (Appendix A). Each data point represents the spleen of an individual mouse processed independently (biological replicate). The number of events acquired per sample and per gate for the short-term study at day 89 pi is reported in Table A1, while the corresponding data for the study at day 190 pi are detailed in Table A2.

2.6. Statistical Analyses

Data were analyzed using non-parametric statistics, as normal distribution could not be reliably assumed due to the small sample sizes per group. Comparisons between more than two groups were performed using the Kruskal–Wallis test followed by Dunn's post-test. For histopathological evaluation (cardiac inflammation and myocardial fibrosis), pairwise effect sizes were calculated using Rosenthal's r ($r = |Z|/\sqrt{N}$) to complement Dunn's post-test (Table A3). For cardiac parasite load, a sensitivity analysis applied the Benjamini–Hochberg false discovery rate procedure (Q = 5%) to the same comparisons, and effect sizes are reported as Hodges–Lehmann median differences with exact confidence intervals from pairwise Mann–Whitney tests (Table A4). Associations between immune and disease parameters were evaluated with Spearman's rank correlation at the individual-animal level, with Benjamini–Hochberg adjustment (Table A5). Analyses were performed using GraphPad Instat 4.0. Differences were considered significant at $p < 0.05$. Data are presented as mean ± SEM with individual data points plotted to show the complete distribution.

The experimental unit was an individual animal. Sample sizes were determined empirically based on previous experimental models and cage capacity without a priori sample size calculation. No animals or data were excluded from the analyses. Group allocation was randomized; thus, treatment allocation concealment was not performed. Investigators were not blinded during the conduct of the experiment, animal handling, or the administration of treatments. Outcome assessments (histopathological scoring of myocardial inflammation and fibrosis, as well as electrocardiographic trace interpretations) were performed in a blinded manner, with samples and recordings identified solely by coded numbers. Data analysis and statistical testing were not conducted blindly.

3. Results

3.1. Short-Term Benznidazole Treatment Acts as an Immunomodulator and Reduces Early Cardiac Parasite Load in a Proof-of-Concept Study

To determine whether a single 7-day short course of BZL or single-agent vaccination could elicit a measurable biological response prior to its integration into a dual-round sequential scheme, an exploratory proof-of-concept study was performed at 89 days post-infection (pi).

3.1.1. Parasite Burden and Humoral Immune Response

Cardiac *T. cruzi* DNA persistence evaluated by qPCR revealed overall low parasite loads across all experimental groups at day 89 pi. Nevertheless, short-course BZL monotherapy (BZL* group) achieved a statistically significant reduction in myocardial parasite load compared to infected-untreated controls (Tc*) ($p < 0.01$; Figure 2a). The vaccinated cohort (Vac* group) showed a numerical decrease in parasite load relative to the Tc* group, although it did not reach statistical significance ($p = 0.0729$). In parallel, assessment of serum humoral immunity confirmed the immunogenicity of the vaccine formulation, as Vac-treated mice generated significantly elevated anti-TSNt IgG1 and IgG2a antibody titers compared to non-vaccinated controls (Figure A3a,b). Meanwhile, anti-parasite homogenate IgG1 and IgG2a levels remained uniformly elevated across all infected groups (OD/cut-off > 1) without significant intergroup differences at this early time point (Figure A3c,d).

3.1.2. Splenic T Cell Population and Functional Profile

To characterize the cellular immune response, absolute numbers of T lymphocyte subpopulations in the spleen were evaluated. Flow cytometric analysis revealed numerically higher absolute cell counts in treated cohorts relative to infected controls. Specifically, short-course BZL treatment significantly increased the total number of $CD4^+$ T cells compared to the Tc* group ($p < 0.05$; Figure 2c). Functional characterization of $CD4^+$ T cells showed distinct modulation depending on the therapeutic regimen: TSNt-ISPA immunization significantly enhanced the number of IFN-γ-producing $CD4^+$ T cells (Figure 2e), whereas BZL treatment induced significant increases in both IFN-γ^+ and regulatory IL-10^+ $CD4^+$ T cell subpopulations (Figure 2e,f). Regarding $CD8^+$ T cells, although total $CD8^+$ cell numbers remained comparable between groups, assessment of cytotoxic potential demonstrated a significant increase in $CD8^+$ $CD107a^+$ T cells in the BZL-treated group compared to Tc* controls ($p < 0.05$; Figure 2i).

3.2. Sequential Chemo-Immunotherapy Protects Against Heart Pathology and Parasite Persistence in the Chronic Phase

Myocardial tissue integrity was evaluated by analyzing the extent of inflammatory infiltrates and collagen deposition/fibrosis. Representative images of each experimental group (40× magnification) are presented in Figure 3a. Generally, the tissue alterations observed in this chronic model were categorized as mild to moderate. To validate the experimental model, the infected-untreated group (Tc) was first compared against the healthy control (NI), demonstrating that chronic infection induced significant increases in both fibrosis levels (Figure 3b) and inflammatory infiltrates (Figure 3c).

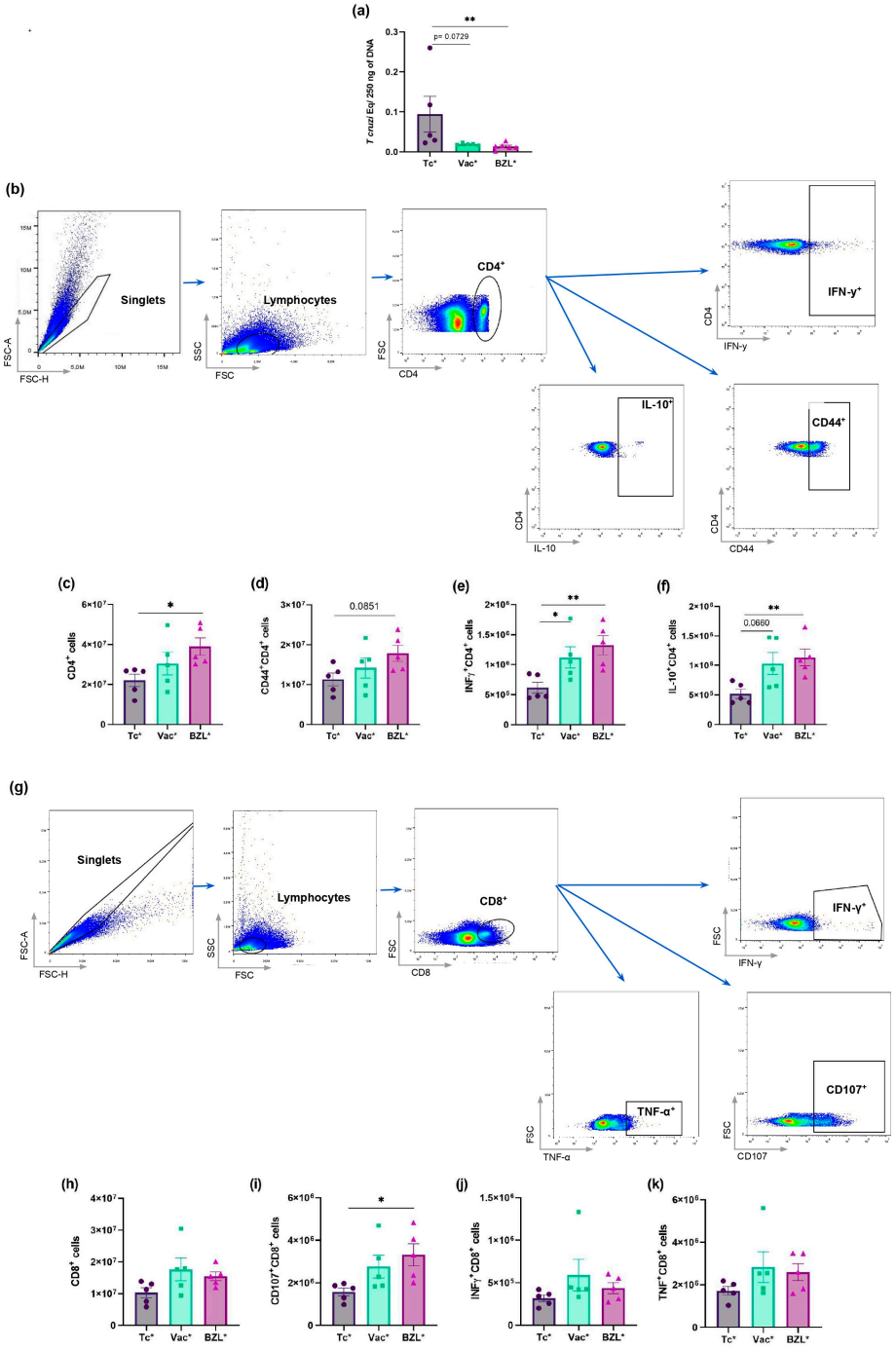


Figure 2. Short-term BZL treatment reduces early cardiac parasite load and modulates splenic T-cell responses in chronic *T. cruzi* infection. (**a**) Cardiac tissue parasite load quantified by qPCR at 89 days post-infection (pi) in infected-untreated control (Tc*), benznidazole monotherapy (BZL*), and therapeutic vaccine monotherapy (Vac*) groups. (**b**–**k**) Flow cytometric characterization of splenic T-cell-mediated cellular immunity following in vitro restimulation with *T. cruzi* total homogenate in co-culture with activated dendritic cells at the experimental endpoint: (**b**) Representative gating strategy for $CD4^+$ T-cell analysis; (**c**) number of total helper $CD4^+$ T cells; (**d**) number of activated $CD4^+CD44^+$ T cells; number of (**e**) IFN-γ and (**f**) IL-10 cells within the $CD4^+$ population; (**g**) representative gating strategy for $CD8^+$ T-cell analysis; (**h**) number of total cytotoxic $CD8^+$ T cells; (**i**) number of degranulating $CD8^+CD107a^+$ T cells; and number of (**j**) IFN-γ and (**k**) TNF-α cells within the $CD8^+$ population. Each point represents an individual animal (n = 5–6 per group), and bars indicate mean ± standard error of the mean (SEM) for each experimental cohort. Cytometric analyses were performed using FlowJo software. Statistical significance is indicated as: * $p < 0.05$, ** $p < 0.01$.

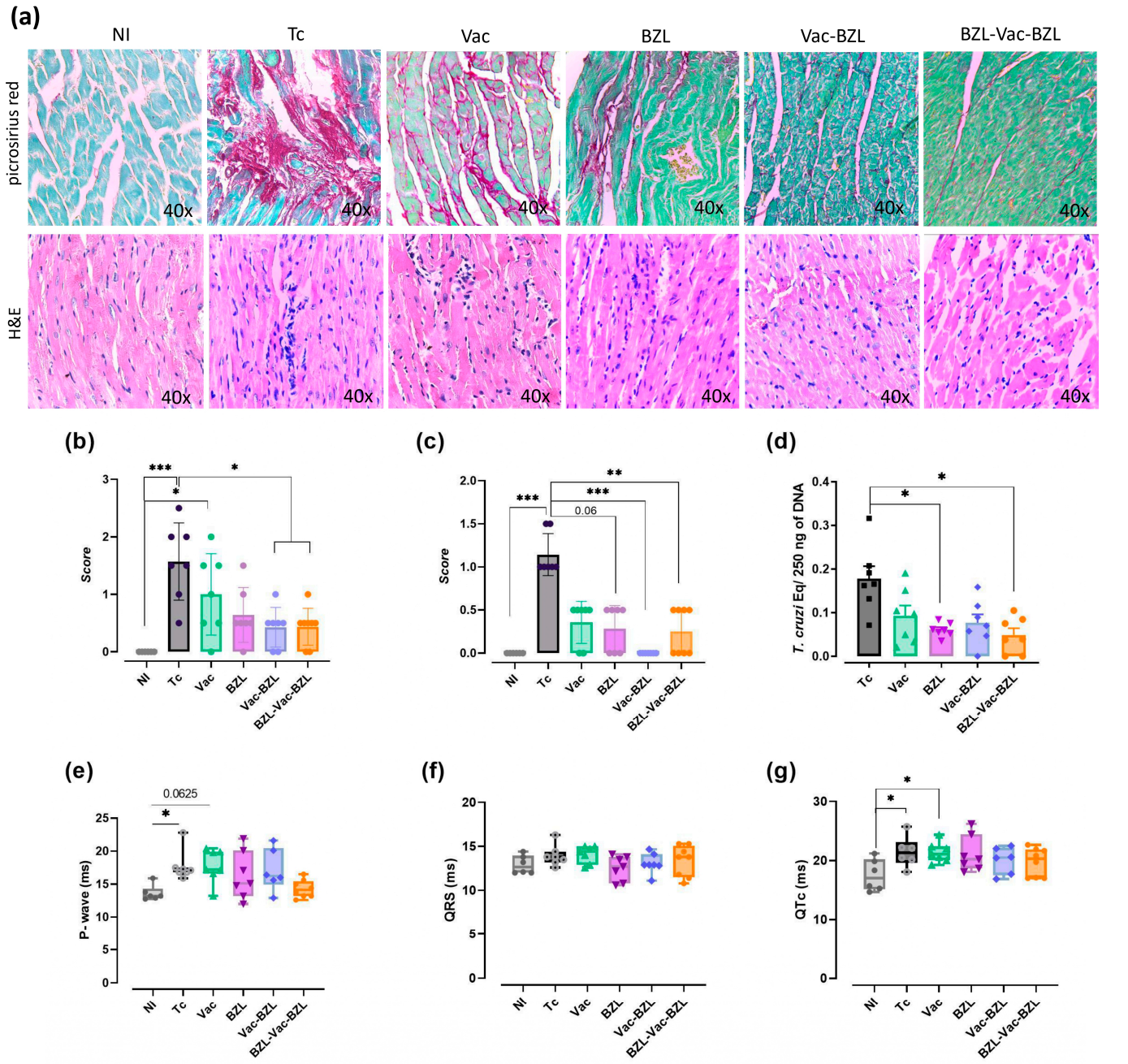


Figure 3. Assessment of myocardial histopathology, cardiac parasite burden, and electrocardiographic parameters in chronic *T. cruzi* infection. (**a**) Representative histological images (40× magnification) of cardiac sections. In Picrosirius Red staining, green indicates muscle cytoplasm and red indicates collagen fibers; in H&E staining, blue indicates nuclear staining and pink indicates cellular cytoplasm. (**b**) Myocardial fibrosis score determined by Picrosirius Red staining. (**c**) Inflammatory infiltrate score evaluated by hematoxylin and eosin (H&E) staining. (**d**) Cardiac parasite load determined via qPCR at 190 days post-infection (pi). (**e**) P-wave duration. (**f**) QRS complex duration. (**g**) Corrected QT interval (QTc) expressed in milliseconds (ms). Panels (**b**–**d**): mean ± SEM. Panels (**e**–**g**): box plots show the median, interquartile range and range; individual dots indicate values from individual animals (n = 6–8 per group). Statistical significance is indicated as * $p < 0.05$, ** $p < 0.01$, and *** $p < 0.001$.

Regarding the analysis of fibrosis (Figure 3b), the infected-untreated group (Tc) exhibited a significant increase in collagen deposition scores compared to the healthy control (NI), registering the highest values of the study (Table A3). Likewise, the Vac group showed a significant increase in this parameter compared to the NI control. In contrast, the combined

regimens Vac → BZL and BZL → Vac → BZL significantly reduced these levels compared to the infected control. Although the groups treated with the monotherapies (Vac and BZL) showed lower fibrosis values compared to the Tc group, these differences did not reach statistical significance against the other experimental groups (Table A3).

The presence of inflammatory infiltrates exhibited a similar pattern (Figure 3c). The Tc group presented a significantly higher degree of inflammation compared to the NI control, and significant differences were also found against the Vac → BZL, and BZL → Vac → BZL groups. Notably, in the Vac → BZL group, all animals displayed normal tissue architecture, completely lacking detectable inflammatory infiltrates.

In parallel, the persistence of *T. cruzi* DNA in cardiac tissue was determined via qPCR at day 190 pi (Figure 3d). Consistent with the low-grade alterations observed in tissues, parasite loads remained at low levels across all analyzed conditions (Figure 3d). When assessing the impact of the different interventions, all applied therapeutic regimens reduced the parasite load compared to the infected control group (Tc). However, this reduction reached statistical significance only in the group treated with benznidazole monotherapy (BZL group) and the sequential regimen group (BZL → Vac → BZL) ($p < 0.05$). Notably, within this latter group, two animals had no detectable parasite load in the myocardial tissue. For detailed pairwise comparisons, effect sizes, and multiple-comparison corrections, see Table A4.

To determine whether these structural and parasitological improvements translated into functional protection, cardiac electrical activity was evaluated by ECG at day 190 pi. Analysis of P-wave duration (Figure 3e) revealed a significant increase in the Tc group compared to non-infected controls (NI). The Vac group exhibited a numerical increase in P-wave duration relative to the NI group ($p = 0.0625$), whereas the sequential treatment group (BZL → Vac → BZL) showed no significant differences relative to the NI group and displayed the lowest data dispersion among all evaluated cohorts. Furthermore, no significant differences were observed in the PR interval among the experimental groups ($p > 0.05$). Conversely, no significant variations were detected in QRS complex duration across any experimental condition (Figure 3f). Regarding the corrected QT interval (QTc) (Figure 3g), a significant prolongation was observed in both the Tc and Vac groups compared to the NI group, suggesting altered ventricular repolarization in these animals. Importantly, direct comparisons among the treated groups revealed no statistically significant differences, reflecting overlapping ranges and individual variability.

3.3. Sequential BZL → Vac → BZL Regimen Induces a Th1-Associated Specific Antibody Response

The capacity of the different protocols to induce a response specifically directed against the vaccine antigen was determined by quantifying anti-TSNt antibodies. Generally, total IgG levels (Figure 4a) reflected the average behavior of the evaluated isotypes, showing values above the positivity threshold (OD/cut-off > 1) in all groups that received the vaccine formulation (Vac, Vac → BZL, and BZL → Vac → BZL).

In all vaccinated groups, the IgG2a isotype (Figure 4c) predominated over IgG1 (Figure 4b), a distinction that was much more pronounced in the sequential BZL–Vac–BZL regimen. In this group, the response leaned markedly toward IgG2a, with IgG2a levels reaching the highest levels observed among all cohorts. Concurrently, its IgG1 levels remained near the cut-off limit (representing the lowest values among the immunized mice) and showed no significant differences compared to negative controls. Conversely, the Vac → BZL group exhibited its most distinctive behavior in IgG2a, where it registered the lowest reactivity among the immunized mice, failing to show significant differences against the non-vaccinated groups. These findings suggest that, although all regimens induce a

Th1-associated humoral profile, the sequential BZL → Vac → BZL scheme results in the most pronounced IgG2a predominance.

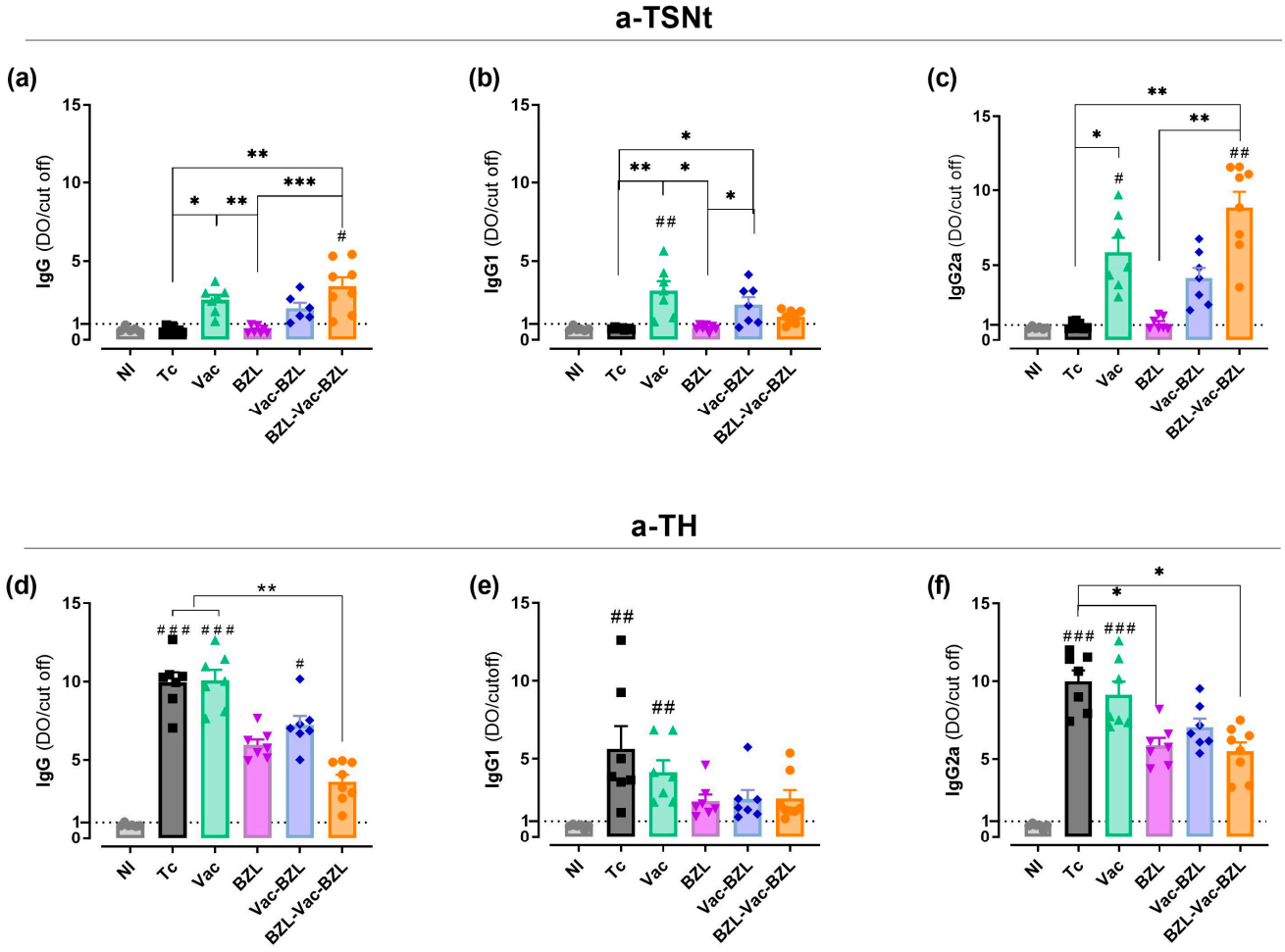


Figure 4. Evaluation of systemic immune response following sequential treatment in the intradermal infection model. Antibody responses were evaluated during the chronic phase of infection after the respective treatments. Anti-TSNt antibody responses are shown for total IgG (**a**), IgG1 (**b**), and IgG2a (**c**). Anti-homogenate (a-TH) responses were also evaluated for total IgG (**d**), IgG1 (**e**), and IgG2a (**f**). Antibody levels are indicated as the optical density (OD) relative to the ELISA cut-off value. Data represent mean ± SEM, with individual dots indicating values from individual animals (n = 6–8 per group). Statistical significance among infected groups is indicated as: * $p < 0.05$, ** $p < 0.01$, and *** $p < 0.001$. Significant differences in each group relative to the non-infected control group (NI) are indicated as: # $p < 0.05$, ## $p < 0.01$, and ### $p < 0.001$.

In a complementary analysis, the humoral response against the total parasite homogenate (TH) was evaluated during the chronic phase of infection. All infected groups showed antibody reactivity above the positivity threshold (OD/cut-off > 1) (Figure 4d–f). Overall, the response was characterized by a predominance of total IgG (Figure 4d) and IgG2a (Figure 4f), both displaying higher magnitudes than IgG1 (Figure 4e). Despite these differences in magnitude, the intergroup pattern remained consistent across all three evaluated markers. The Tc and Vac groups showed the highest antibody reactivity against TH, displaying significantly higher levels of total IgG (Figure 4d), IgG1 (Figure 4e), and IgG2a (Figure 4f) than the non-infected (NI) control. In contrast, groups receiving benznidazole showed lower antibody reactivity, particularly for total IgG and IgG2a. Total IgG levels were significantly lower in the sequential BZL → Vac → BZL group than in Tc and Vac (Figure 4d). For IgG2a, both BZL monotherapy and the BZL → Vac → BZL regimen resulted

in significantly lower levels than the Tc group (Figure 4f). No significant differences among infected groups were detected for IgG1 (Figure 4e).

3.4. Sequential BZL → Vac → BZL Treatment Modulates Cardiac Cytokine and Transcription Factor Profiles Toward Balanced Immunoregulation

To characterize the local immune response within the myocardial tissue, the relative mRNA expression of key cytokines and master transcription factors was evaluated by RT-qPCR.

Regarding the cytokine profile, IL-10 expression levels (Figure 5a) were significantly increased in the Vac, BZL, and BZL → Vac → BZL groups compared with non-infected controls (NI). Conversely, IFN-γ mRNA levels (Figure 5b) showed a significant upregulation in the Tc and Vac groups relative to the NI group, with the Vac group exhibiting significantly higher levels than the BZL monotherapy cohort. In the case of IL-17 (Figure 5c), no statistically significant differences were detected among any of the experimental groups; however, numerical values were higher in the NI and BZL → Vac → BZL groups, with individual animals presenting undetectable values across all cohorts.

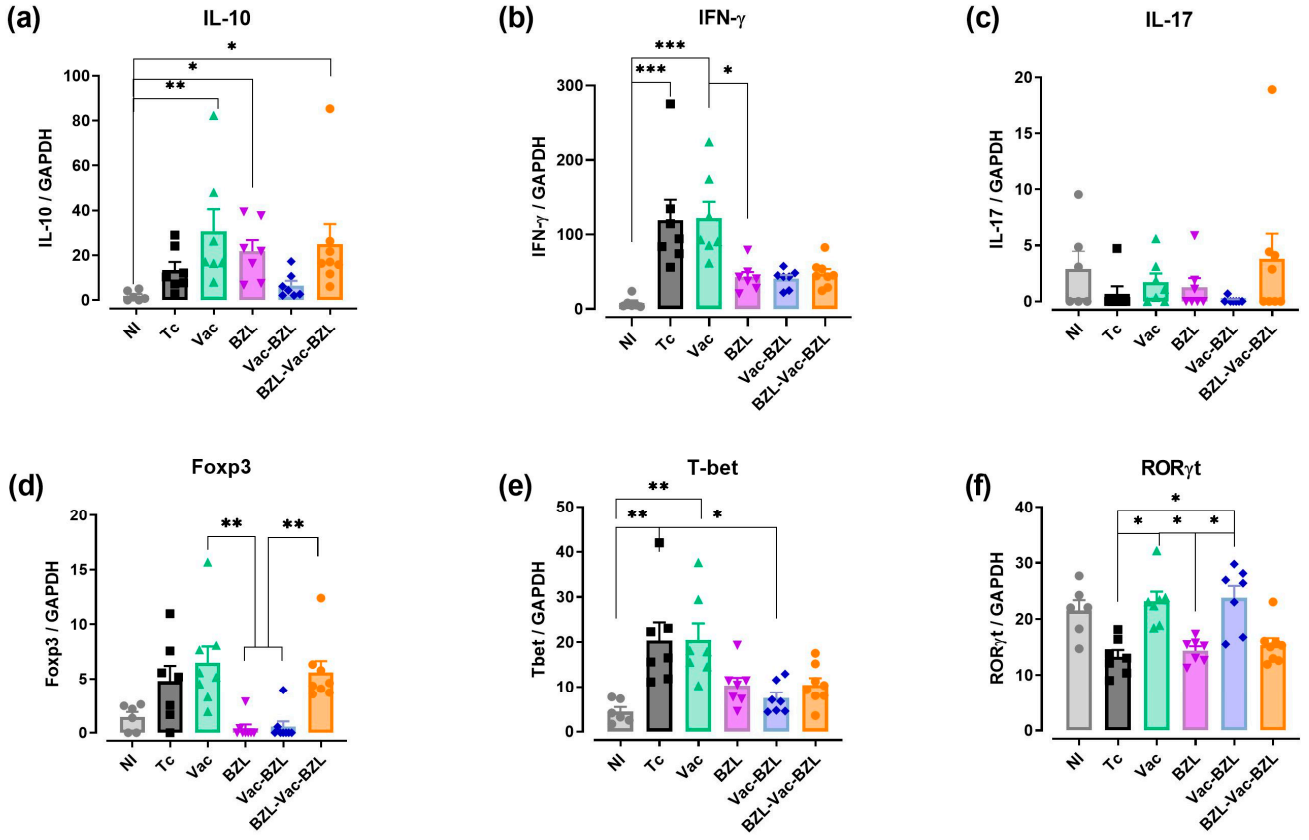


Figure 5. Relative mRNA expression of cytokines and transcription factors in cardiac tissue from animals treated with the sequential regimen in the intradermal infection model. Relative mRNA expression levels determined by RT-qPCR for cytokines (**a**) IL-10, (**b**) IFN-γ, and (**c**) IL-17, and transcription factors (**d**) Foxp3, (**e**) T-bet, and (**f**) RORγt in cardiac tissue across experimental groups. Data represent relative gene expression mean ± SEM, with individual dots indicating values from individual animals (n = 6–8 per group). Statistically significant differences between groups are indicated by comparison bars (* $p < 0.05$, ** $p < 0.01$, *** $p < 0.001$).

The analysis of lineage-specific master transcription factors revealed that Foxp3 expression (Figure 5d) was significantly elevated in the Vac and sequential BZL → Vac → BZL groups compared to the BZL and Vac → BZL groups. On the other hand, T-bet expression (Figure 5e) was significantly increased in the Tc and Vac groups compared with the NI group, with levels in the Vac group being significantly higher than those in the Vac → BZL group. Finally, RORγt mRNA expression (Figure 5f) was significantly increased in the Vac and Vac → BZL groups relative to the Tc and BZL groups, whereas the NI group displayed elevated baseline values without reaching statistical significance compared to the other experimental cohorts.

3.5. Sequential BZL → Vac → BZL Scheme Potentiates Regulatory CD4$^+$ T Cells and Antigen-Specific CD8$^+$ Effector Responses

To characterize the antigen-specific cellular response, splenocytes were restimulated in vitro with TH in the presence of DCs. Following 15 h of stimulation, cellular subpopulations were characterized via flow cytometry.

Regarding the CD4$^+$ T cell population, gated as depicted in Figure 6a, a significant increase in the percentage of these cells (Figure 6b) was observed in the Vac and Vac → BZL groups compared to the Tc control group. When analyzing the activation status via CD44 expression (Figure 6c), the BZL → Vac → BZL group showed a significant increase compared to the Vac group, as well as a higher value than the NI control that did not reach statistical significance ($p = 0.0793$). Regarding the effector cytokine profile, IFN-γ-producing CD4$^+$ T cells (Figure 6d) increased in the Vac group compared to the NI and BZL groups. Concurrently, the sequential group was numerically higher compared to the NI control, but the difference was not statistically significant ($p = 0.0825$). Finally, the regulatory response was analyzed through IL-10-producing CD4$^+$ T cells (Figure 6e). In this parameter, the sequential group stood out notably, showing an increase compared to all experimental groups, achieving statistical significance against Tc, Vac, and BZL.

The CD8$^+$ T cell subpopulation was evaluated under the same stimulation conditions following the gating hierarchy illustrated in Figure 6f. Unlike the observations in the CD4$^+$ population, the total percentage of CD8$^+$ T cells (Figure 6g) did not show significant variations among the different experimental groups. However, relevant differences were detected when evaluating the cytotoxic capacity and functional profile of these cells. Regarding the expression of the degranulation marker CD107a (Figure 6h), the group treated with BZL monotherapy showed a significant increase relative to the NI, Tc, and Vac groups. On the other hand, when analyzing proinflammatory cytokine production, TNF-α-producing CD8$^+$ T cells (Figure 6i) showed an increased percentage within the BZL → Vac → BZL group, reaching statistical significance compared to the NI and Tc controls. Finally, no significant differences were recorded among groups for IFN-γ production (Figure 6j) within this cellular subpopulation.

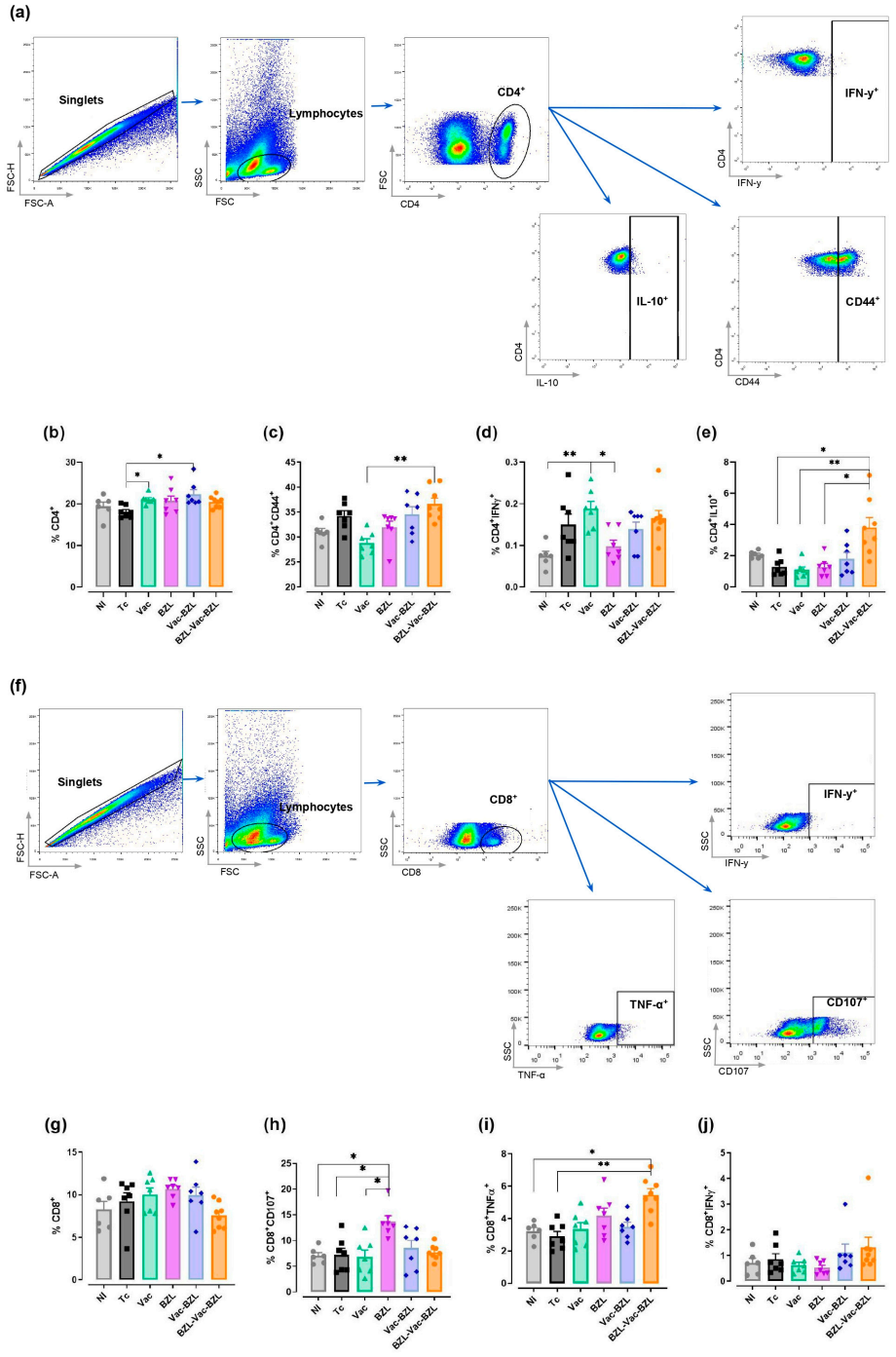


Figure 6. Evaluation of T-cell mediated cellular immune response in splenocytes from animals treated with the sequential regimen in the intradermal infection model. Splenocytes were harvested at the end of the experimental protocol and restimulated in vitro with *T. cruzi* homogenate in co-culture with activated dendritic cells. (**a**) Representative gating strategy for the analysis of the $CD4^+$ population; frequencies of (**b**) total T helper cells ($CD4^+$) and (**c**) activated T helper cells ($CD4^+CD44^+$); percentage of (**d**) IFN-γ-producing and (**e**) IL-10-producing cells within the $CD4^+$ population. (**f**) Representative gating strategy for the analysis of the $CD8^+$ population; percentage of (**g**) total cytotoxic T cells ($CD8^+$) and (**h**) degranulating T cells ($CD8^+CD107a^+$), and intracellular production of (**i**) TNF-α and (**j**) IFN-γ by $CD8^+$ T cells. Bars represent the percentage (%) of positive cells within each specific population (gated cells), expressed as the mean ± standard error of the mean (SEM) for each experimental group, with individual dots indicating values from individual animals (n = 6–8 per group). Data analysis was performed using FlowJo software. Statistical significance levels are indicated as: * $p < 0.05$, ** $p < 0.01$.

4. Discussion

The potential of chemoimmunotherapy for the treatment of chronic Chagas disease has been explored in a limited number of studies, with evidence that this approach can reduce the required dose of BZL and improve cardiac outcomes in experimental infections [17,19,38]. In one of these studies, our group used a chronic infection model in which BALB/c mice remained parasite-positive in blood and tissues despite receiving 30 days of BZL treatment during the chronic stage. In this study we reported that administration of the TSNt-ISPA vaccine before BZL treatment reduced tissue parasite burden and attenuated histological and electrocardiographic alterations associated with cardiac damage [17]. The promising results obtained by our group and others indicate that further studies are needed to determine the optimal timing and sequencing of combined treatments.

In the present study, we hypothesized that the beneficial immunomodulatory effects of BZL [21–23,39] could enhance the efficacy of this treatment strategy when administered as a sequential drug → vaccine → drug regimen. We also aimed to shorten the duration of BZL treatment, to avoid adverse effects associated with this drug. Therefore, we investigated whether a 7-day BZL treatment could be sufficient to enhance the immune response in comparison with therapeutic vaccination. Using our chronic BALB/c model of infection, the 7-day shortened regimen of benznidazole (100 mg/kg/day; BZL* group) exerted a measurable therapeutic effect, significantly reducing cardiac parasite load compared to untreated infected controls (Tc*). This finding suggests that even a brief exposure window can achieve a therapeutic effect locally in the myocardium, consistent with pharmacokinetic reports of limited tissue biodistribution [40].

At the cellular level, this short course increased T-cell responses more markedly than therapeutic vaccination. Splenic cytokine profiles in this group corroborated this homeostatic balance: the expansion of $CD4^+$ IFN-γ^+ and $CD8^+$ $CD107a^+$ cells indicated Th1 commitment, while the concomitant rise in $CD4^+$ IL-10^+ cells suggested the induction of regulatory counter-mechanisms that limit immunopathological collateral damage once parasite replication is curtailed [39]. These observations suggest a functional restoration of T-cell competence, aligning with prior evidence that links the reduction in chronic antigenic load to the recovery of lymphocyte homeostasis [21,39].

Single-agent vaccination (Vac*) was also immunogenic, elevating $CD4^+$ IFN-γ^+ frequencies and showing a numerical, non-significant decrease in cardiac parasite burden ($p = 0.0729$). However, the superior performance of the shortened BZL regimen led us to investigate whether its effects could enhance the efficacy of a subsequent therapeutic vaccination.

Building on these proof-of-concept findings, we subsequently designed and evaluated the long-term sequential chemo-immunotherapeutic protocol (BZL → Vac → BZL) through day 190 pi. This full sequential scheme, integrating short-term chemotherapy with therapeutic immunization, significantly lowered myocardial parasite burden at day 190 pi—a finding reinforced by pairwise comparisons and multiple-comparison corrections showing significant reductions versus the infected control group (Table A4). Parasite DNA fell below qPCR detection limits in some subjects which is an outcome not achieved with BZL monotherapy in our chronic infection model. Furthermore, it provided superior protection against structural myocardial damage and functional electrical disturbances. This biological benefit was linked to a Th1-associated humoral response (IgG2a), the expansion of activated splenic IL-10-producing $CD4^+$ T cells, and an increase in functional TNF-α-producing $CD8^+$ T cells.

As described above, Bustamante and Tarleton [11] proposed that parasite control benefits from intermittent pulses disrupting active rounds of intracellular replication rather than continuous chemical exposure due to the biological dynamics of dormant or qui-

escent amastigotes. These non-proliferative forms reduce metabolic activity and evade nitroheterocyclic prodrugs that require activation by parasite-encoded nitroreductases [10]. Spacing two short cycles of BZL apart likely allowed quiescent amastigotes to re-enter an active replicative cycle during the drug-free interval, rendering them susceptible to the subsequent round of chemotherapy. Here we determined cardiac parasite loads below the limit of detection in two of eight animals from the sequential BZL → Vac → BZL group but not the BZL group, which may be explained by the host immune response boosted by the intervening vaccine added to the proposed intermittent BZL treatment described by Bustamante and Tarleton [11]. Although these findings are exploratory and require confirmation in independent experiments, they represent a promising result. Reducing the duration of benznidazole treatment is a particularly important goal strongly advocated by the medical community involved in Chagas disease management [41].

Regarding structural integrity, combined regimens (Vac → BZL and BZL → Vac → BZL) were the only interventions capable of significantly attenuating myocardial collagen deposition and inflammatory infiltrates relative to infected controls (Tc) with large effect sizes (Table A3), an outcome that monotherapies (BZL, Vac) failed to achieve with statistical significance. These results parallel findings by Dzul-Huchim and Jones [19,38], who observed that combined approaches protect cardiac architecture using low drug doses, outperforming single-agent treatments. The preservation of tissue architecture directly correlated with enhanced electrophysiological stability: all evaluated treatments were associated with reduction in the P-wave prolongation observed in the infected control group, whereas QTc intervals remained largely unaffected by BZL-containing regimens. Prolonged QTc duration reflects impaired ventricular repolarization that may be driven by ion channel remodeling and disrupted connexin-mediated gap junctions, which collectively establish an arrhythmogenic substrate for re-entrant circuits [37,42,43].

Humoral responses revealed pronounced IgG2a polarization in the sequential group, matching the levels achieved by vaccine monotherapy. This suggests that prior BZL administration does not compromise the immunogenicity of subsequent vaccination. Moreover, protocols incorporating more than one intervention successfully reduced anti-parasite homogenate titers (total IgG and IgG2a), whereas vaccine monotherapy failed to lower anti-homogenate reactivity. This behavior is consistent with a reduction in parasite load. A possible shift in the antibody repertoire could also contribute to the improved efficacy of the treatment, although this possibility remains to be investigated in future studies. Notably, in an oral infection model, nasal monotherapy with TSNt adjuvanted with c-di-AMP significantly reduced anti-homogenate antibodies [35], suggesting that both the route of parasite entry and the vaccine formulation may influence the humoral response.

At the cellular level, flow cytometry demonstrated that TSNt immunization, administered alone, expanded $CD4^+$ T-cell frequencies and IFN-γ production. This confirms the immunogenic potency of the TSNt-ISPA formulation and its capacity to sustain Th1 activation even in an established chronic infection as reported previously for other therapeutic vaccines [19,20,44].

Importantly, the sequential scheme was the only regimen that promoted a substantial expansion of splenic IL-10-producing $CD4^+$ T cells, suggesting a pivotal counter-regulatory mechanism that mitigates bystander tissue injury, a delicate balance that clinically distinguishes indeterminate from cardiopathic patients [45–47]. Within the $CD8^+$ compartment, only the sequential protocol increased the frequency of TNF-α-producing $CD8^+$ T cells. Because the early loss of TNF-α expression is a defining hallmark of hierarchical T cell exhaustion in chronic infections [48,49], its functional restoration reflects the recovery of effector competence, in line with observations by Dzul-Huchim et al. [19] for combination immunotherapy. Notably, only mice receiving BZL monotherapy exhibited increased

CD107a expression, a hallmark of cytotoxic degranulation that has been linked to tissue damage in chronic murine *T. cruzi* infection [50]. While an initial, transient cytotoxic activation can favor early parasite reduction—as observed in our short-term trial—its uncontrolled persistence promotes ongoing myocardial injury. Consistent with this, patients with CCC display elevated CD107a/b expression on $CD8^+$ T cells, indicating an enhanced cytotoxic potential during chronic infection [47,51]. Therefore, the increase in TNF-α-producing $CD8^+$ T cells in the absence of elevated CD107a expression may represent a favorable outcome, reflecting an increase in a specific effector function without concomitant activation of cytotoxic degranulation.

These systemic findings are corroborated locally by transcriptional analysis of the myocardial microenvironment (Section 3.4/Figure 5), where the BZL → Vac → BZL cohort showed upregulated cardiac expression of IL-10 and Foxp3, in stark contrast to the untreated infected and vaccine-monotherapy groups, which exhibited predominant IFN-γ and T-bet expression. This local modulation aligns with the increase in splenic $CD4^+$ IL-10^+ T cells, suggesting that the immunoregulatory phenotype induced by the sequential protocol operates directly within the heart tissue, reinforcing the mechanistic link between immunoregulation and myocardial preservation.

Collectively, these data highlight treatment-specific immune specialization: BZL monotherapy primarily fosters cytotoxic responsiveness, vaccination drives humoral-Th1 polarization, and the sequential BZL → Vac → BZL regimen uniquely integrates both effector arms under IL-10- and Foxp3-mediated immunoregulation, verified both systemically and in cardiac tissue. Although these findings are associations and were not tested for causality in this model, this controlled activation profile represents an optimal therapeutic objective for Chagas disease, potentially providing sustained control over persistent parasite reservoirs while halting progression toward chronic chagasic cardiomyopathy.

It is worth noting that individual-animal correlation analyses across treatment groups revealed consistently negative Spearman correlation coefficients between the evaluated immune parameters (IgG2a/IgG1 ratios against TS and TH, and the frequencies of $CD4^+$ IL-10+ and $CD8^+$ TNF-α+ T cells) and disease parameters (parasite burden, fibrosis, and inflammation). Although some of these associations showed moderate correlation coefficients and nominal *p*-values below 0.05, none remained statistically significant after adjustment for multiple comparisons using the Benjamini–Hochberg false discovery rate (BH-FDR) procedure. These results suggest a possible association between these immune parameters and more favorable disease outcomes, although this relationship should be interpreted cautiously and requires further investigation (Table A5).

Some limitations of the present study should be acknowledged. First, the small group sizes limit statistical power and increase the risk of type II errors, so non-significant differences should be interpreted with caution. In addition, each group was housed in a single cage, so cage effects cannot be separated from treatment effects. Future studies should include larger sample sizes to increase statistical power and strengthen the robustness of the findings. It will also be important to evaluate the therapeutic strategy against different *T. cruzi* strains and DTUs. In this regard, our previous study evaluated the vaccine strategy using DTU I and DTU VI parasites [17], providing a basis for extending the present findings to additional parasite backgrounds.

Another limitation is that the present study was performed using a single sex. Although protection induced by this antigen has previously been demonstrated in a prophylactic vaccination model [52], that study revealed sex-dependent differences in the immune response. Such differences could potentially influence the outcome of therapeutic vaccination during chronic infection. Therefore, including both male and female animals will be necessary to determine whether sex influences the efficacy and immunological mechanisms of the

sequential treatment regimen. Furthermore, longer follow-up periods and more advanced stages of chronic infection should be investigated to determine whether the beneficial effects of the sequential treatment are maintained over time and whether this strategy can provide long-term protection against the progressive cardiac alterations associated with chronic *T. cruzi* infection.

Our design also did not include a BZL → Vac group, so we cannot separate the effect of treatment order from that of the combination itself. Cumulative benznidazole exposure was matched between the BZL and sequential groups, which supports a contribution of the vaccine, but the specific role of sequence remains to be tested.

Electrocardiograms were recorded under ketamine–xylazine anesthesia, which depresses heart rate and can alter cardiac conduction in mice. In a comparison of anesthetics in mice, ketamine–xylazine caused more marked bradycardia than pentobarbital-based protocols, although it had fewer effects on heart rate variability parameters [53]. Since all groups received the same protocol, comparisons between groups remain informative, but absolute values may differ from those in conscious animals or under other anesthetics.

In addition, treatment administration and data analysis, including flow cytometry gating, were not performed blindly, which may introduce observer bias despite the standardized procedures and the blinded histopathological and electrocardiographic assessments. Blinding at these stages will be incorporated in subsequent experiments.

Finally, we recently found that a nasal formulation of the same antigen adjuvanted with c-di-AMP conferred protection as a stand-alone therapeutic vaccine in a chronic oral-infection model—an effect not achieved by TSNt-ISPA monotherapy in the present model—and notably induced a tissue Th17-type response that was absent here [35]. These differences, likely driven by the distinct infection route, adjuvant, and immunization route, suggest that mucosal delivery engages complementary immune mechanisms worth exploring in combination with the sequential BZL → Vac → BZL regimen evaluated in this study.

5. Conclusions

Our findings support the potential of a sequential BZL → Vac → BZL regimen as an improved therapeutic strategy for chronic Chagas disease in this murine model. This approach achieved superior control of myocardial parasite burden and provided greater protection against cardiac structural and electrical alterations than monotherapies or single combined therapy. These effects were associated with increased TNF-α-producing $CD8^+$ T-cell responses, together with enhanced immunoregulatory mechanisms. Further studies are warranted to validate this strategy in different experimental settings and stages of chronic infection.

Author Contributions: Conceptualization, P.C., A.R.P. and I.S.M.; methodology, P.C., E.P., M.F.P., A.R.P. and I.S.M.; investigation, P.C., E.P., U.C., M.F.P., C.B.B., B.D., G.F.D., F.B.G. and C.F.; data curation, P.C., E.P., U.C., M.F.P., A.R.P. and I.S.M.; formal analysis, P.C., E.P., M.F.P., A.R.P. and I.S.M.; writing—original draft preparation, P.C. and I.S.M.; writing—review and editing, P.C., M.F.P., A.R.P. and I.S.M.; supervision, I.S.M. All authors have read and agreed to the published version of the manuscript.

Funding: This research was supported by the Argentine National Agency for the Promotion of Science and Technology (ANPCyT; grants PICT-2021-I-A-01235, PICT 2018-03462 and PICT-2021-I-A-01026), CAI+D 2020 PI Tipo II (Code 50620190100075LI), CONICET PIP 0715, PID-UNR 2022 (80020210200052UR), and PID-UNR 1MED516.

Institutional Review Board Statement: The animal study protocol was approved by the Advisory Committee of Ethics and Research Safety (CAESI) of the Facultad de Bioquímica y Ciencias Biológicas, Universidad Nacional del Litoral (UNL), Argentina (protocol code CE2018-42).

Informed Consent Statement: Not applicable.

Data Availability Statement: The data supporting the findings of this study, are available within the article and its appendix. The raw data supporting the conclusions of this article will be made available by the authors, without undue reservation. The experimental protocol is available at the laboratory but was not prospectively registered in a publicly accessible repository.

Acknowledgments: The authors acknowledge the support of the Argentine National Agency for the Promotion of Science and Technology (ANPCyT), the National Scientific and Technical Research Council (CONICET), the National University of the Littoral (Universidad Nacional del Litoral, UNL), and the National University of Rosario (Universidad Nacional de Rosario, UNR).

Conflicts of Interest: The authors declare no conflicts of interest.

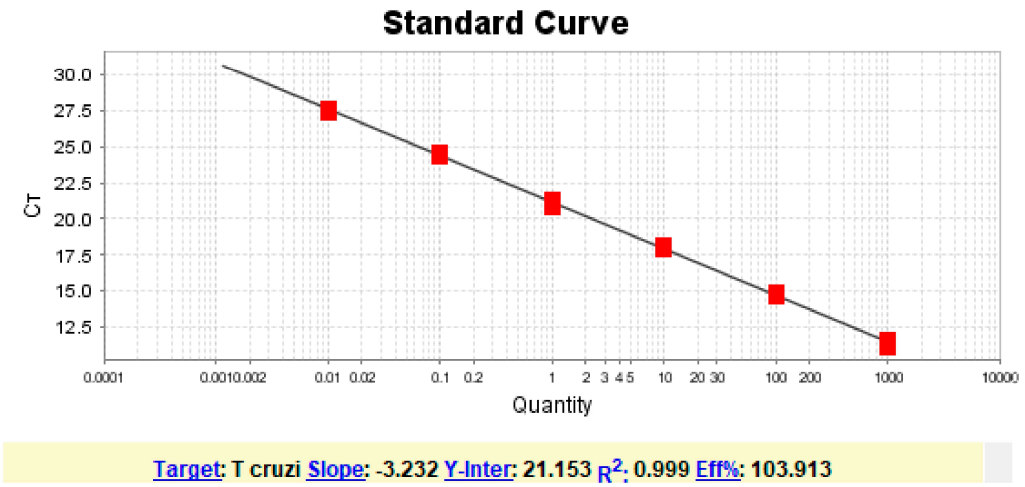
Abbreviations

The following abbreviations are used in this manuscript:

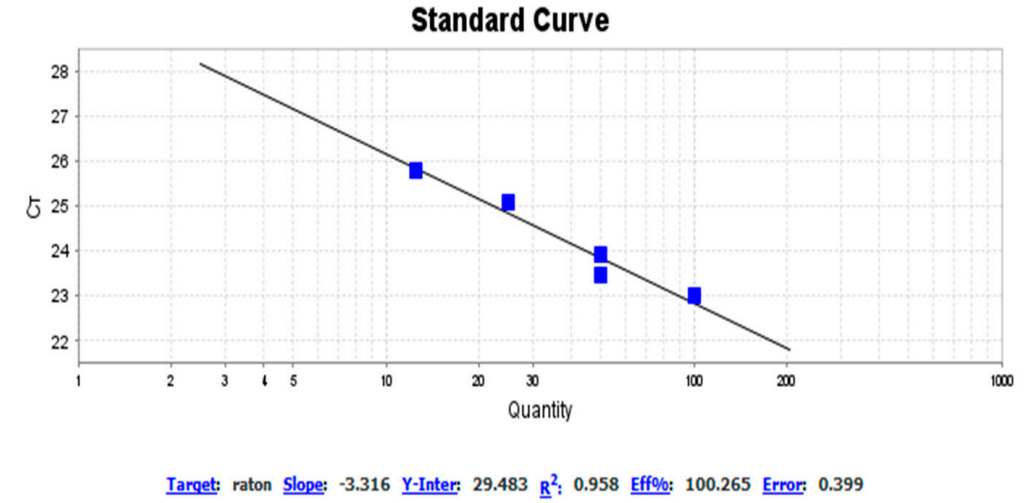
BCA	Bicinchoninic acid
BSA	Bovine serum albumin
BZL	Benznidazole
CCC	Chronic Chagas cardiomyopathy
Ct	Threshold cycle
c-di-AMP	Bis-(3′,5′)-cyclic dimeric adenosine monophosphate
DCs	Dendritic cells
DNA	Deoxyribonucleic acid
DTU	Discrete typing unit
ECG	Electrocardiogram
EDTA	Ethylenediaminetetraacetic acid
ELISA	Enzyme-linked immunosorbent assay
FBS	Fetal bovine serum
FDR	False discovery rate
FMO	Fluorescence-minus-one
Foxp3	Forkhead box P3
H&E	Hematoxylin and eosin
IFN-γ	Interferon-gamma
IgG	Immunoglobulin G
IL-10	Interleukin 10
IL-17a	Interleukin 17a
IPTG	Isopropyl β-D-1-thiogalactopyranoside
ISPA	Immunostimulant particles
kDNA	Kinetoplast deoxyribonucleic acid
LOD	Limit of detection
MWCO	Molecular weight cut-off
Ni-NTA	Nickel-nitrilotriacetic acid
PBS	Phosphate-buffered saline
pi	Post-infection
qPCR	Quantitative real-time polymerase chain reaction
QTc	Corrected QT interval
RORγt	Retinoic acid receptor-related orphan receptor gamma t
RPMI	Roswell Park Memorial Institute [medium]
RT-qPCR	Reverse transcription quantitative real-time polymerase chain reaction
SAPA	Shed acute phase antigen
SDS	Sodium dodecyl sulfate
SDS-PAGE	Sodium dodecyl sulfate–polyacrylamide gel electrophoresis
SEM	Standard error of the mean
T-bet	T-box transcription factor expressed in T cells
TH	*Trypanosoma cruzi* total homogenate
TMB	3,3′,5,5′-Tetramethylbenzidine
TNF-α	Tumor necrosis factor-alpha
TSNt	Amino-terminal fragment of *Trypanosoma cruzi* trans-sialidase

Appendix A

Appendix A.1. Quantification of Cardiac Parasite Load by qPCR



(**a**)



(**b**)

Figure A1. Standard curves for the quantification of *T. cruzi* DNA and murine DNA by qPCR. (**a**) Standard curve for *T. cruzi* kDNA (primers S36/S67rev). Ct values are plotted against the log10 of the amount of *T. cruzi* equivalents per reaction (range: 0.01 to 1000). (**b**) Standard curve for murine DNA (TNF-α gene) [range: 12.5 to 100 ng per reaction]. Each point represents an individual replicate and the line shows the linear regression. Slope, coefficient of determination (R^2) and amplification efficiency are indicated in each panel. The limit of detection (LOD) of the *T. cruzi* assay, defined as the lowest concentration amplified in all replicates, was 0.01 equivalents per reaction (Ct 27.40 and 27.68; 2/2 replicates).

Appendix A.2. Flow Cytometry Controls and Event Counts

Table A1. Flow cytometry event counts and gated frequencies of splenic T-cell populations in the short-term study at day 89 pi.

Population (Gate)	Tc*		BZL*		Vac*	
	Events	% of Parent	Events	% of Parent	Events	% of Parent
Total events acquired	355,684 (351,358–357,915)	100	352,300 (338,503–356,027)	100	356,071 (207,337–429,494)	100
$CD4^+$	43,598 (31,918–47,519)	19.2 (16.1–21.5)	49,471 (38,901–54,496)	23.0 (19.9–26.1)	40,771 (16,918–54,841)	20.1 (17.0–22.4)
$CD4^+CD44^+$	14,697 (13,412–22,504)	36.6 (31.3–47.4)	16,130 (15,635–18,638)	34.2 (29.2–40.2)	13,402 (6151–20,341)	36.4 (31.6–40.9)
$CD4^+$IFN-γ^+	853 (570–955)	1.99 (1.31–2.43)	1237 (1023–1249)	2.49 (2.07–2.76)	1095 (640–1249)	2.62 (2.00–3.78)
$CD4^+$IL-10^+	415 (340–494)	0.93 (0.78–1.39)	672 (427–833)	1.30 (0.86–1.66)	507 (469–999)	1.23 (1.06–3.00)
$CD8^+$	17,167 (15,104–19,733)	8.11 (6.69–8.28)	16,394 (14,379–20,664)	7.79 (7.46–9.51)	18,441 (8999–19,838)	9.53 (7.00–9.78)
$CD8^+CD107a^+$	1480 (1214–1579)	8.11 (7.09–8.98)	1627 (1480–1839)	10.50 (7.87–12.80)	1648 (1123–1878)	9.02 (8.37–12.50)
$CD8^+$TNF-α^+	552 (434–601)	2.9 (2.47–4.91)	567 (419–952)	3.78 (2.44–5.81)	433 (389–674)	3.65 (1.96–4.64)
$CD8^+$IFN-γ^+	85 (61–119)	0.48 (0.36–0.66)	86 (51–99)	0.56 (0.25–0.65)	93 (44–103)	0.49 (0.46–0.58)

Values are median (min–max) per mouse. Events: number of events in each gate. % of parent: frequency relative to the immediately preceding gate. Each sample corresponds to the spleen of one mouse, seeded in a single well, after in vitro restimulation with *T. cruzi* total homogenate and activated dendritic cells. $n = 5$ (Tc*), 6 (BZL*) and 5 (Vac*).

Table A2. Number of events acquired and gated for each splenocyte population at day 190 pi.

Population (Gate)	NI	Tc	BZL	Vac	Vac → BZL	BZL → Vac → BZL
Total events acquired	100,000 (85,495–146,811)	100,000 (68,076–460,773)	199,930 (62,650–284,560)	100,000 (85,410–251,150)	171,421 (99,711–253,550)	140,616.5 (86,250–338,061)
$CD4^+$	11,554 (5581–13,666)	13,762 (7288–51,852)	21,046 (6978–42,840)	14,183 (8846–35,518)	22,323 (13,605–32,656)	18,919 (11,106–46,577)
$CD4^+CD44^+$	3908 (1563–4490)	4801 (2678–17,304)	7167 (2365–10,617)	4226 (2309–9541)	8747 (4192–11,847)	7079 (3762–16,038)
$CD4^+$IFN-γ^+	10.5 (2–24)	21 (13–63)	18 (4–52)	26 (13–69)	38 (10–56)	24 (8–96)
$CD4^+$IL-10^+	219 (119–1066)	167 (95–845)	186 (140–457)	132 (87–618)	310 (179–741)	771 (170–1442)
$CD8^+$	4221.5 (2950–22,245)	6176 (1445–29,959)	7555 (3433–29,759)	5295 (4862–25,712)	16,762 (1633–19,793)	10,173.5 (1886–21,888)
$CD8^+CD107a^+$	269.5 (173–2851)	259 (186–2422)	1492 (408–4302)	228 (128–2253)	1942 (53–2512)	612 (195–1574)
$CD8^+$TNF-α^+	140.5 (101–728)	158 (111–866)	483 (101–1276)	208 (102–976)	564 (41–795)	531 (123–1143)
$CD8^+$IFN-γ^+	73 (20–150)	84 (27–102)	52 (23–94)	48 (31–119)	99 (4–503)	126 (34–238)

Values are median (range) of events per sample, $n = 6$ (NI), 7 (Tc, BZL, Vac, Vac → BZL) and 8 (BZL → Vac → BZL). Each sample corresponds to the spleen of one mouse, seeded in a single well. Gating strategies are shown in Figure 6a,f. Percentages of positive cells within each parent gate are shown in Figure 6.

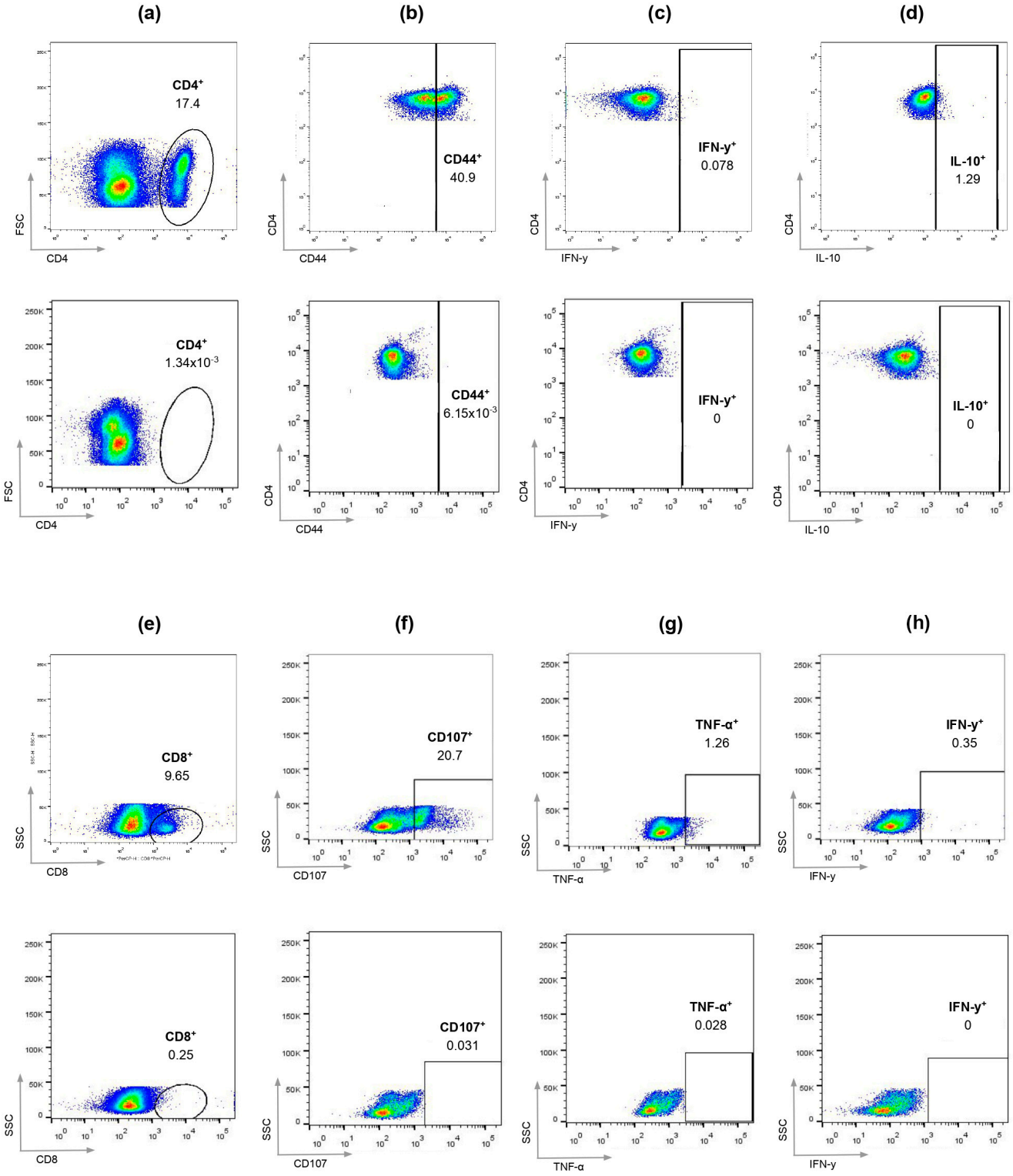


Figure A2. Fluorescence-minus-one (FMO) controls used to set the positivity gates for flow cytometry. Representative dot plots of splenocytes from an NI mouse restimulated in vitro with *T. cruzi* total homogenate and activated dendritic cells. For each gate, the fully stained sample is shown above its FMO control, with the same gate applied to both. (**a**–**d**) $CD4^+$ population: (**a**) $CD4^+$, (**b**) $CD4^+CD44^+$, (**c**) IFN-γ^+ and (**d**) IL-10^+ within $CD4^+$. (**e**–**h**) $CD8^+$ population: (**e**) $CD8^+$, (**f**) $CD8^+CD107a^+$, (**g**) TNF-α^+ and (**h**) IFN-γ^+ within $CD8^+$. FMO controls contained all antibodies of the panel except the one indicated. Gates were set on the FMO control and applied identically to all samples. Numbers indicate the percentage of events within each gate.

Appendix A.3. Statistical Analyses

Table A3. Pairwise comparisons of cardiac inflammation and myocardial fibrosis scores at 190 days post-infection: Dunn's adjusted *p*-values and effect sizes.

Comparison	Inflamm. Adj. *p*	Inflamm. Effect Size (r)	Fibrosis Adj. *p*	Fibrosis Effect Size (r)
Tc vs. Vac	ns	0.66	ns	0.38
Tc vs. BZL	ns (0.06)	0.77	ns	0.57
Tc vs. Vac → BZL	***	1.22	*	0.79
Tc vs. BZL → Vac → BZL	*	0.89	*	0.76
Tc vs. NI	***	1.22	***	1.24
Vac vs. BZL	ns	0.11	ns	0.19
Vac vs. Vac → BZL	ns	0.56	ns	0.41
Vac vs. BZL → Vac → BZL	ns	0.22	ns	0.39
Vac vs. NI	ns	0.56	*	0.86
BZL vs. Vac → BZL	ns	0.45	ns	0.22
BZL vs. BZL → Vac → BZL	ns	0.11	ns	0.20
BZL vs. NI	ns	0.45	ns	0.67
Vac → BZL vs. BZL → Vac → BZL	ns	0.34	ns	0.02
Vac → BZL vs. NI	ns	0.00	ns	0.46
BZL → Vac → BZL vs. NI	ns	0.33	ns	0.47

Kruskal–Wallis test followed by Dunn's post-test. Adjusted *p*-values: ns, $p \geq 0.05$; * $p < 0.05$; *** $p < 0.001$. Effect sizes were calculated using Rosenthal's r ($r = |Z|/\sqrt{N}$, where $N = n_1 + n_2$). Values of $r \geq 0.10$, $r \geq 0.30$, and $r \geq 0.50$ indicate small, medium, and large effect sizes, respectively.

Table A4. Cardiac parasite load at 190 days post-infection: pairwise comparisons with effect sizes and multiple-comparison correction.

Comparison	Median Difference (95% CI)	Adjusted *p* (Dunn)	q-Value (FDR, BH)
BZL-Vac-BZL vs. Vac	0.03928 (−0.01898 to 0.1066)	>0.9999	0.4924
BZL-Vac-BZL vs. BZL	0.01102 (−0.02547 to 0.05186)	>0.9999	0.7447
BZL-Vac-BZL vs. Vac-BZL	0.02525 (−0.02806 to 0.07721)	>0.9999	0.5702
BZL-Vac-BZL vs. Tc	0.1235 (0.06055 to 0.1912)	0.0078	0.0078
Vac vs. BZL	−0.02898 (−0.09925 to 0.03082)	>0.9999	0.6820
Vac vs. Vac-BZL	−0.01528 (−0.09754 to 0.05592)	>0.9999	0.8391
Vac vs. Tc	0.08649 (7.300×10^{-5} to 0.1652)	0.3306	0.0826
BZL vs. Vac-BZL	0.01201 (−0.02872 to 0.06332)	>0.9999	0.7447
BZL vs. Tc	0.1102 (0.05623 to 0.1562)	0.0448	0.0224
Vac-BZL vs. Tc	0.09550 (0.01676 to 0.1656)	0.1958	0.0653

Median difference (95% CI) refers to the Hodges–Lehmann estimate of the difference between medians. Confidence intervals are not adjusted for multiple comparisons. Adjusted *p* values were calculated using Dunn's post-test following a significant Kruskal–Wallis test. q-values were adjusted using the Benjamini–Hochberg (BH) procedure (Q = 5%) to control the False Discovery Rate (FDR). The NI group was excluded because non-infected animals carry no parasite DNA. Samples below the limit of detection were assigned a value of zero. Analyses were performed in GraphPad Instat 4.0.

Table A5. Correlations between immune parameters and disease outcomes in infected mice.

Immune Parameter	Outcome	Spearman rho	95% CI	*p*	Adjusted *p* (BH-FDR)
IgG2a/IgG1 (TSNt)	Parasite burden	−0.11	−0.43 to 0.23	0.513	0.559
IgG2a/IgG1 (TSNt)	Fibrosis	−0.32	−0.59 to 0.02	0.060	0.172
IgG2a/IgG1 (TSNt)	Inflammation	−0.28	−0.57 to 0.06	0.094	0.188
IgG2a/IgG1 (TH)	Parasite burden	−0.06	−0.39 to 0.29	0.744	0.744
IgG2a/IgG1 (TH)	Fibrosis	−0.17	−0.48 to 0.18	0.333	0.499
IgG2a/IgG1 (TH)	Inflammation	−0.18	−0.49 to 0.17	0.287	0.492
$CD4^+$ IL-10^+	Parasite burden	−0.12	−0.44 to 0.23	0.495	0.559
$CD4^+$ IL-10^+	Fibrosis	−0.14	−0.45 to 0.21	0.431	0.559
$CD4^+$ IL-10^+	Inflammation	−0.34	−0.61 to −0.01	0.039	0.172
$CD8^+$ TNF-α^+	Parasite burden	−0.30	−0.58 to 0.04	0.072	0.172
$CD8^+$ TNF-α^+	Fibrosis	−0.36	−0.62 to −0.02	0.031	0.172
$CD8^+$ TNF-α^+	Inflammation	−0.31	−0.58 to 0.04	0.070	0.172

Spearman correlations between immune parameters and disease outcomes in infected animals ($n = 36$). TSNt: trans-sialidase; TH: total parasite homogenate. *p* values are unadjusted; adjusted *p* values were calculated with the Benjamini–Hochberg false discovery rate (FDR) method across the 12 comparisons shown. CI: confidence interval.

Appendix A.4. Antibody Responses in the Short-Term Study

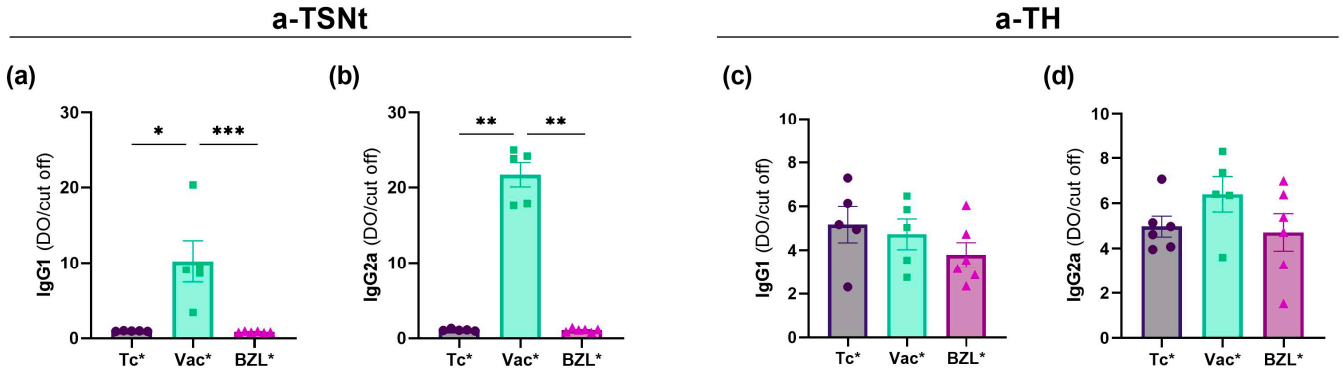


Figure A3. Evaluation of serum antibody responses to individual vaccine or benznidazole treatments for scheme optimization. Antibody responses were assessed during the chronic phase of infection following the respective monotherapies. Anti-TSNt (a-TSNt) antibody responses were evaluated for (**a**) IgG1 and (**b**) IgG2a. The anti-homogenate (a-TH) antibody response was likewise assessed for (**c**) IgG1 and (**d**) IgG2a. Antibody levels are indicated as the optical density (OD) relative to the ELISA cut-off value (OD/cut-off). Data represent mean ± SEM, with individual dots indicating values from individual animals (n = 5–6 per group). Statistical significance is indicated as: * $p < 0.05$, ** $p < 0.01$, and *** $p < 0.001$.

References

1. World Health Organization. Chagas Disease (American Trypanosomiasis). 2023. Available online: https://www.who.int/chagas/en/ (accessed on 11 November 2026).
2. Ferreira, M.d.S.; Maldonado, R.A.; Farani, P.S.G. Chagas Disease in the 21st Century: Global Spread, Ecological Shifts, and Research Frontiers. *Biology* **2025**, *14*, 1631. [CrossRef] [PubMed]
3. Montalvo-Ocotoxtle, I.G.; Rojas-Velasco, G.; Rodríguez-Morales, O.; Arce-Fonseca, M.; Baeza-Herrera, L.A.; Arzate-Ramírez, A.; Meléndez-Ramírez, G.; Manzur-Sandoval, D.; Lara-Romero, M.L.; Reyes-Ortega, A.; et al. Chagas Heart Disease: Beyond a Single Complication, from Asymptomatic Disease to Heart Failure. *J. Clin. Med.* **2022**, *11*, 7262. [CrossRef] [PubMed]
4. Lewis, M.D.; Fortes Francisco, A.; Taylor, M.C.; Burrell-Saward, H.; McLatchie, A.P.; Miles, M.A.; Kelly, J.M. Bioluminescence Imaging of Chronic *Trypanosoma cruzi* Infections Reveals Tissue-Specific Parasite Dynamics and Heart Disease in the Absence of Locally Persistent Infection. *Cell. Microbiol.* **2014**, *16*, 1285–1300. [CrossRef] [PubMed]
5. Jones, K.; Versteeg, L.; Damania, A.; Keegan, B.; Kendricks, A.; Pollet, J.; Cruz-Chan, J.V.; Gusovsky, F.; Hotez, P.J.; Bottazzi, M.E. Vaccine-Linked Chemotherapy Improves Benznidazole Efficacy for Acute Chagas Disease. *Infect. Immun.* **2018**, *86*, e00876-17. [CrossRef] [PubMed]
6. Campos, M.C.O.; Leon, L.L.; Taylor, M.C.; Kelly, J.M. Benznidazole-Resistance in *Trypanosoma cruzi*: Evidence That Distinct Mechanisms Can Act in Concert. *Mol. Biochem. Parasitol.* **2014**, *193*, 17–19. [CrossRef] [PubMed]
7. Bern, C. Chagas' Disease. *N. Engl. J. Med.* **2015**, *373*, 456–466. [CrossRef] [PubMed]
8. Viotti, R.; Vigliano, C.; Lococo, B.; Alvarez, M.G.; Petti, M.; Bertocchi, G.; Armenti, A. Side Effects of Benznidazole as Treatment in Chronic Chagas Disease: Fears and Realities. *Expert Rev. Anti-Infect. Ther.* **2009**, *7*, 157–163. [CrossRef] [PubMed]
9. Mejia, A.M.; Hall, B.S.; Taylor, M.C.; Gómez-Palacio, A.; Wilkinson, S.R.; Triana-Chávez, O.; Kelly, J.M. Benznidazole-Resistance in *Trypanosoma cruzi* Is a Readily Acquired Trait That Can Arise Independently in a Single Population. *J. Infect. Dis.* **2012**, *206*, 220–228. [CrossRef] [PubMed]
10. Sánchez-Valdéz, F.J.; Padilla, A.; Wang, W.; Orr, D.; Tarleton, R.L. Spontaneous Dormancy Protects *Trypanosoma cruzi* during Extended Drug Exposure. *eLife* **2018**, *7*, e34039. [CrossRef] [PubMed]
11. Bustamante, J.M.; Sanchez-Valdez, F.; Padilla, A.M.; White, B.; Wang, W.; Tarleton, R.L. A Modified Drug Regimen Clears Active and Dormant Trypanosomes in Mouse Models of Chagas Disease. *Sci. Transl. Med.* **2020**, *12*, eabb7656. [CrossRef] [PubMed]
12. Martín-Escolano, J.; Medina-Carmona, E.; Martín-Escolano, R. Chagas Disease: Current View of an Ancient and Global Chemotherapy Challenge. *ACS Infect. Dis.* **2020**, *6*, 2830–2843. [CrossRef] [PubMed]

13. Dumonteil, E.; Herrera, C. Vaccines against Chronic *Trypanosoma cruzi* Infection: Progress, Challenges and Future Directions. *Expert Rev. Vaccines* **2026**, *25*, 2632658. [CrossRef] [PubMed]
14. Puerta, C.J.; Cuellar, A.; Lasso, P.; Mateus, J.; Gonzalez, J.M. *Trypanosoma cruzi*-Specific CD8$^+$ T Cells and Other Immunological Hallmarks in Chronic Chagas Cardiomyopathy: Two Decades of Research. *Front. Cell. Infect. Microbiol.* **2022**, *12*, 1075717. [CrossRef] [PubMed]
15. Pérez-Antón, E.; Egui, A.; Thomas, M.C.; Carrilero, B.; Simón, M.; López-Ruz, M.Á.; Segovia, M.; López, M.C. A Proportion of CD4$^+$ T Cells from Patients with Chronic Chagas Disease Undergo a Dysfunctional Process, Which Is Partially Reversed by Benznidazole Treatment. *PLoS Negl. Trop. Dis.* **2021**, *15*, e0009059. [CrossRef] [PubMed]
16. Castro Eiro, M.D.; Natale, M.A.; Alvarez, M.G.; Shen, H.; Viotti, R.; Lococo, B.; Bua, J.; Nuñez, M.; Bertocchi, G.L.; Albareda, M.C.; et al. Reduced *Trypanosoma cruzi*-Specific Humoral Response and Enhanced T Cell Immunity after Treatment Interruption with Benznidazole in Chronic Chagas Disease. *J. Antimicrob. Chemother.* **2021**, *76*, 1580–1592. [CrossRef] [PubMed]
17. Prochetto, E.; Bontempi, I.; Rodeles, L.; Cabrera, G.; Vicco, M.; Cacik, P.; Pacini, M.F.; Pérez Gianeselli, M.; Pérez, A.R.; Marcipar, I. Assessment of a Combined Treatment with a Therapeutic Vaccine and Benznidazole for the *Trypanosoma cruzi* Chronic Infection. *Acta Trop.* **2022**, *229*, 106334. [CrossRef] [PubMed]
18. Cruz-Chan, J.V.; Villanueva-Lizama, L.E.; Versteeg, L.; Damania, A.; Villar, M.J.; González-López, C.; Keegan, B.; Pollet, J.; Gusovsky, F.; Hotez, P.J.; et al. Vaccine-Linked Chemotherapy Induces IL-17 Production and Reduces Cardiac Pathology during Acute *Trypanosoma cruzi* Infection. *Sci. Rep.* **2021**, *11*, 3222. [CrossRef] [PubMed]
19. Dzul-Huchim, V.M.; Ramirez-Sierra, M.J.; Martinez-Vega, P.P.; Rosado-Vallado, M.E.; Arana-Argaez, V.E.; Ortega-Lopez, J.; Gusovsky, F.; Dumonteil, E.; Cruz-Chan, J.V.; Hotez, P.; et al. Vaccine-Linked Chemotherapy with a Low Dose of Benznidazole plus a Bivalent Recombinant Protein Vaccine Prevents the Development of Cardiac Fibrosis Caused by *Trypanosoma cruzi* in Chronically-Infected BALB/c Mice. *PLoS Negl. Trop. Dis.* **2022**, *16*, e0010258. [CrossRef] [PubMed]
20. Nguyen, D.M.; Poveda, C.; Pollet, J.; Gusovsky, F.; Bottazzi, M.E.; Hotez, P.J.; Jones, K.M. The Impact of Vaccine-Linked Chemotherapy on Liver Health in a Mouse Model of Chronic *Trypanosoma cruzi* Infection. *PLoS Negl. Trop. Dis.* **2023**, *17*, e0011519. [CrossRef] [PubMed]
21. Bustamante, J.M.; Bixby, L.M.; Tarleton, R.L. Drug-Induced Cure Drives Conversion to a Stable and Protective CD8$^+$ T Central Memory Response in Chronic Chagas Disease. *Nat. Med.* **2008**, *14*, 542–550. [CrossRef] [PubMed]
22. Egui, A.; López, M.C.; Gómez, I.; Simón, M.; Segovia, M.; Thomas, M.C. Differential Phenotypic and Functional Profile of Epitope-Specific Cytotoxic CD8$^+$ T Cells in Benznidazole-Treated Chronic Asymptomatic Chagas Disease Patients. *Biochim. Biophys. Acta (BBA)—Mol. Basis Dis.* **2020**, *1866*, 165629. [CrossRef] [PubMed]
23. Mateus, J.; Pérez-Antón, E.; Lasso, P.; Egui, A.; Roa, N.; Carrilero, B.; González, J.M.; Thomas, M.C.; Puerta, C.J.; López, M.C.; et al. Antiparasitic Treatment Induces an Improved CD8$^+$ T Cell Response in Chronic Chagasic Patients. *J. Immunol.* **2017**, *198*, 3170–3180. [CrossRef] [PubMed]
24. Laucella, S.A.; Mazliah, D.P.; Bertocchi, G.; Alvarez, M.G.; Cooley, G.; Viotti, R.; Albareda, M.C.; Lococo, B.; Postan, M.; Armenti, A.; et al. Changes in *Trypanosoma cruzi*-Specific Immune Responses after Treatment: Surrogate Markers of Treatment Efficacy. *Clin. Infect. Dis.* **2009**, *49*, 1675–1684. [CrossRef] [PubMed]
25. Michailowsky, V.; Murta, S.M.; Carvalho-Oliveira, L.; Pereira, M.E.; Ferreira, L.R.; Brener, Z.; Romanha, A.J.; Gazzinelli, R.T. Interleukin-12 Enhances in Vivo Parasiticidal Effect of Benznidazole during Acute Experimental Infection with a Naturally Drug-Resistant Strain of *Trypanosoma cruzi*. *Antimicrob. Agents Chemother.* **1998**, *42*, 2549–2556. [CrossRef] [PubMed]
26. Romanha, A.J.; Alves, R.O.; Murta, S.M.F.; Silva, J.S.; Ropert, C.; Gazzinelli, R.T. Experimental Chemotherapy against *Trypanosoma cruzi* Infection: Essential Role of Endogenous Interferon-Gamma in Mediating Parasitologic Cure. *J. Infect. Dis.* **2002**, *186*, 823–828. [CrossRef] [PubMed]
27. Pacini, M.F.; Bulfoni Balbi, C.; Dinatale, B.; Farré, C.; Cacik, P.; Gonzalez, F.B.; Marcipar, I.; Pérez, A.R. Intranasal Trans-Sialidase Vaccine Mitigates Acute and Chronic Pathology in a Preclinical Oral Chagas Disease Model. *Vaccines* **2024**, *12*, 1171. [CrossRef] [PubMed]
28. Bontempi, I.A.; Vicco, M.H.; Cabrera, G.; Villar, S.R.; González, F.B.; Roggero, E.A.; Ameloot, P.; Callewaert, N.; Pérez, A.R.; Marcipar, I.S. Efficacy of a Trans-Sialidase-ISCOMATRIX Subunit Vaccine Candidate to Protect against Experimental Chagas Disease. *Vaccine* **2015**, *33*, 1274–1283. [CrossRef] [PubMed]
29. Garcia, S.; Ramos, C.O.; Senra, J.F.V.; Vilas-Boas, F.; Rodrigues, M.M.; Campos-de-Carvalho, A.C.; Ribeiro-dos-Santos, R.; Soares, M.B.P. Treatment with Benznidazole during the Chronic Phase of Experimental Chagas' Disease Decreases Cardiac Alterations. *Antimicrob. Agents Chemother.* **2005**, *49*, 1521–1528. [CrossRef] [PubMed]
30. Saeftel, M.; Fleischer, B.; Hoerauf, A. Stage-Dependent Role of Nitric Oxide in Control of *Trypanosoma cruzi* Infection. *Infect. Immun.* **2001**, *69*, 2252–2259. [CrossRef] [PubMed]

31. Chatelain, E.; Konar, N. Translational Challenges of Animal Models in Chagas Disease Drug Development: A Review. *Drug Des. Dev. Ther.* **2015**, *9*, 4807–4823. [CrossRef] [PubMed]
32. Penitente, A.R.; Leite, A.L.J.; de Paula Costa, G.; Shrestha, D.; Horta, A.L.; Natali, A.J.; Neves, C.A.; Talvani, A. Enalapril in Combination with Benznidazole Reduces Cardiac Inflammation and Creatine Kinases in Mice Chronically Infected with *Trypanosoma cruzi*. *Am. J. Trop. Med. Hyg.* **2015**, *93*, 976–982. [CrossRef] [PubMed]
33. Scarim, C.B.; Ribeiro, A.R.; Rosa, J.A.d.; Chin, C.M. Response to Different Benznidazole Doses in Animal Models of Chronic Phase Chagas Disease: A Critical Review. *Rev. Soc. Bras. Med. Trop.* **2018**, *51*, 133–140. [CrossRef] [PubMed]
34. Pacini, M.F.; González, F.B.; Dinatale, B.; Bulfoni Balbi, C.; Villar, S.R.; Farré, C.; Lupi, G.; Espariz, M.; Blancato, V.S.; Magni, C.; et al. Nasal Immunization with a *L. lactis*-Derived Trans-Sialidase Antigen plus c-Di-AMP Protects against Acute Oral *T. cruzi* Infection. *Vaccine* **2022**, *40*, 2311–2323. [CrossRef] [PubMed]
35. Cacik, P.; Pacini, M.F.; Bulfoni Balbi, C.; Dinatale, B.; Diaz, G.; Cha, U.; Farré, C.; Gianeselli, M.; Prochetto, E.; Peréz, A.R.; et al. Nasal Vaccination against *Trypanosoma cruzi*: A Dual Approach for Prevention and Treatment of Chronic Chagas Cardiomyopathy. *Front. Immunol.* **2025**, *16*, 1662036. [CrossRef] [PubMed]
36. Cummings, K.L.; Tarleton, R.L. Rapid Quantitation of *Trypanosoma cruzi* in Host Tissue by Real-Time PCR. *Mol. Biochem. Parasitol.* **2003**, *129*, 53–59. [CrossRef] [PubMed]
37. Mitchell, G.F.; Jeron, A.; Koren, G. Measurement of Heart Rate and Q-T Interval in the Conscious Mouse. *Am. J. Physiol.* **1998**, *274*, H747–H751. [CrossRef] [PubMed]
38. Jones, K.M.; Mangin, E.N.; Reynolds, C.L.; Villanueva, L.E.; Cruz, J.V.; Versteeg, L.; Keegan, B.; Kendricks, A.; Pollet, J.; Gusovsky, F.; et al. Vaccine-Linked Chemotherapy Improves Cardiac Structure and Function in a Mouse Model of Chronic Chagas Disease. *Front. Cell. Infect. Microbiol.* **2023**, *13*, 1106315. [CrossRef] [PubMed]
39. Acevedo, G.R.; Girard, M.C.; Gómez, K.A. The Unsolved Jigsaw Puzzle of the Immune Response in Chagas Disease. *Front. Immunol.* **2018**, *9*, 1929. [CrossRef] [PubMed]
40. Perin, L.; Moreira da Silva, R.; Fonseca, K.d.S.; Cardoso, J.M.d.O.; Mathias, F.A.S.; Reis, L.E.S.; Molina, I.; Correa-Oliveira, R.; Vieira, P.M.d.A.; Carneiro, C.M. Pharmacokinetics and Tissue Distribution of Benznidazole after Oral Administration in Mice. *Antimicrob. Agents Chemother.* **2017**, *61*, e02410-16. [CrossRef] [PubMed]
41. Pan American Health Organization. *Guía Para el Diagnóstico y el Tratamiento de la Enfermedad de Chagas*, 2nd ed.; Pan American Health Organization: Washington, DC, USA, 2026.
42. Roman-Campos, D.; Marin-Neto, J.A.; Santos-Miranda, A.; Kong, N.; D'Avila, A.; Rassi, A. Arrhythmogenic Manifestations of Chagas Disease: Perspectives From the Bench to Bedside. *Circ. Res.* **2024**, *134*, 1379–1397. [CrossRef] [PubMed]
43. Ferreira, R.R.; de Souza, E.M.; Vilar-Pereira, G.; Degrave, W.M.S.; Abreu, R.d.S.; Meuser-Batista, M.; Ferreira, N.V.C.; Ledbeter, S.; Barker, R.H.; Bailly, S.; et al. In Chagas Disease, Transforming Growth Factor Beta Neutralization Reduces *Trypanosoma cruzi* Infection and Improves Cardiac Performance. *Front. Cell. Infect. Microbiol.* **2022**, *12*, 1017040. [CrossRef] [PubMed]
44. Delfino, M.A.; Trinitario, S.; Cenizo, R.; Carrizo, F.; Borgo, J.; Dzvonyk, P.; Cardoso, A.; Barbieri, I.; Buchholz, B.; Chaneton, L.; et al. mRNA-Tc-Vax Vaccine Induces T Cell-Dependent Prophylactic and Therapeutic Protection Against *Trypanosoma cruzi*. *Res. Sq.* **2025**, *preprint*. [CrossRef] [PubMed]
45. Cristovão-Silva, A.C.; Brelaz-de-Castro, M.C.A.; Hernandes, M.Z.; Pereira, V.R.A. Chagas Disease: Immunology of the Disease at a Glance. *Cytokine Growth Factor Rev.* **2021**, *62*, 15–22. [CrossRef] [PubMed]
46. Koh, C.C.; Neves, E.G.A.; de Souza-Silva, T.G.; Carvalho, A.C.; Pinto, C.H.R.; Sobreira Galdino, A.; Gollob, K.J.; Dutra, W.O. Cytokine Networks as Targets for Preventing and Controlling Chagas Heart Disease. *Pathogens* **2023**, *12*, 171. [CrossRef] [PubMed]
47. Neves, E.G.A.; Koh, C.C.; Souza-Silva, T.G.; Passos, L.S.A.; Silva, A.C.C.; Velikkakam, T.; Villani, F.; Coelho, J.S.; Brodskyn, C.I.; Teixeira, A.; et al. T-Cell Subpopulations Exhibit Distinct Recruitment Potential, Immunoregulatory Profile and Functional Characteristics in Chagas versus Idiopathic Dilated Cardiomyopathies. *Front. Cardiovasc. Med.* **2022**, *9*, 787423. [CrossRef] [PubMed]
48. Wherry, E.J. T Cell Exhaustion. *Nat. Immunol.* **2011**, *12*, 492–499. [CrossRef] [PubMed]
49. Gálvez, R.I.; Jacobs, T. Exhausted PD-1^{+} TOX^{+} CD8^{+} T Cells Arise Only in Long-Term Experimental *Trypanosoma cruzi* Infection. *Front. Immunol.* **2022**, *13*, 866179. [CrossRef] [PubMed]
50. Mateus, J.; Guerrero, P.; Lasso, P.; Cuervo, C.; González, J.M.; Puerta, C.J.; Cuéllar, A. An Animal Model of Acute and Chronic Chagas Disease with the Reticulotropic Y Strain of *Trypanosoma cruzi* That Depicts the Multifunctionality and Dysfunctionality of T Cells. *Front. Immunol.* **2019**, *10*, 918. [CrossRef] [PubMed]
51. Lasso, P.; Mateus, J.; Pavía, P.; Rosas, F.; Roa, N.; Thomas, M.C.; López, M.C.; González, J.M.; Puerta, C.J.; Cuéllar, A. Inhibitory Receptor Expression on CD8^{+} T Cells Is Linked to Functional Responses against *Trypanosoma cruzi* Antigens in Chronic Chagasic Patients. *J. Immunol.* **2015**, *195*, 3748–3758. [CrossRef] [PubMed]

52. Bulfoni Balbi, C.; Pacini, M.F.; Dinatale, B.; Farré, C.; Cacik, P.; Prochetto, E.; González, F.B.; Marcipar, I.; Cabrera, G.; Pérez, A.R. Sexual Dimorphism-Driven Differences Are Overcome in a Preclinical Vaccine Model against *Trypanosoma cruzi*. *Front. Immunol.* **2025**, *16*, 1526573. [CrossRef] [PubMed]
53. Kazdağlı, H.; Özel, H.F.; Özbek, M.; Alpay, Ş.; Alenbey, M. Classical Heart Rate Variability and Nonlinear Heart Rate Analysis in Mice under Napentobarbital and Ketamine/Xylazine Anesthesia. *Turk. J. Med. Sci.* **2022**, *52*, 858–869. [CrossRef] [PubMed]

Disclaimer/Publisher's Note: The statements, opinions and data contained in all publications are solely those of the individual author(s) and contributor(s) and not of MDPI and/or the editor(s). MDPI and/or the editor(s) disclaim responsibility for any injury to people or property resulting from any ideas, methods, instructions or products referred to in the content.